Monte Carlo simulations of the Cu3Pd(110) surface using embedded atom method potentials

Brienen, S.G.M.

Award date:
1995

Technische Universiteit Eindhoven
Faculteit der Technische Natuurkunde
Vakgroep Vaste Stof
Onderzoeksgroep Fysica van de Oppervlakken en Grenslagen

Monte Carlo simulations of the $Cu_3Pd(110)$ surface using embedded atom method potentials

Bas Brienen
July 1995

Verslag van afstudeeronderzoek, uitgevoerd in de groep Theoretical and Experimental Physics onder leiding van Prof. dr. H. van Houten aan het Philips Natuurkundig Laboratorium.

Supervision:
Dr. H. Feil (Philips)
Dr. A.W. Denier van der Gon (TUE)

Afstudeerhoogleraar:
Prof. dr. H.H. Brongersma

Abstract

In this work the $Cu_3Pd(110)$ (2×1) surface is investigated. The aim of this study is to describe the surface with embedded atom method (EAM) potential functions using Monte Carlo simulations.

Bulk simulations of the Cu_3Pd crystal show a Cu_3Au ordered structure below a temperature of T~250K. Phase diagrams in literature indicate that the order-disorder transition temperature of the Cu_3Pd bulk is T~730K.

The $Cu_3Pd(110)$ surface was found to have a $Cu_{50}Pd_{50}$ composition in the outermost layer and 100% Cu in the second layer in case the surface is not reconstructed. The $Cu_{50}Pd_{50}$ layer is ordered and shows a (2×1) LEED pattern below a temperature of T~220K. Above a temperature of T~220K the order dissapears and the second layer is enriched with ~5 at.% Pd. This result is in contradiction with LEIS-experiments on a $Cu_{85}Pd_{15}(110)$ (2×1) surface which show ~11 at.% Pd in the outermost layer and ~40at.% in the second layer.

Molecular dynamics simulations have been performed to assign the peaks in the spectrum found in the TOF-SARS experiments on a $Cu_{85}Pd_{15}(110)$ (2×1) . The presence of a peak which was not mentioned in the spectrum indicates that the surface contains a large number of vacancies or other defects.

Monte Carlo simulations to investigate the behaviour of the vacancies in the surface led to two possible surface terminations. First, a missing row reconstructed surface with 100% Cu in the outermost layer and a second layer consisting of ~35at.% Cu and ~65at.% Pd. This possibility is ruled out by TOF-SARS experiments. The other possibility is a stepped surface. The surface termination of a stepped surface is a $Cu_{50}Pd_{50}$ composition in the outermost layer with 100% Cu in the second layer and is in contradiction with LEIS-experiments .

Table of Contents

1. INTRODUCTION

A catalyst is a substance which increases the rate of a chemical reaction, without being consumed. Since most reactants will not penetrate into the bulk of the catalyst only the surface will catalyze the reaction. Therefore the study of surfaces is very important. The investigation of alloy surfaces is interesting because the catalytic properties of an alloy can be different from the compound properties. The goal is to design alloys with the catalytic properties necessary.

Copper and palladium catalysts are efficient for a large number of reactions like oxidation of carbon monoxides and hydrocarbons, selective hydrogenation of carbon monoxide to methanol and reduction of NO_x to N_2. An example is a palladium catalyst used in an automotive three-way catalyst. Recently such a catalyst was developed and commercialized [1]. Copper can also be used for the reactions necessary in an automotive catalyst. The problem using this element is sulfur poisoning. Sulfur poisoning was a smaller problem for a Pd-catalyst and has been overcome by decreasing the sulfur concentration in gasoline. Although Cu and Pd can be used as catalyst for the same reactions, the reaction mechanisms are completely different.

Future generation fuels like reformulated gasoline and alternative fuels (methanol, ethanol and natural gas) will require other catalytic properties. Copper and palladium are promising catalyst for these fuels. Maybe it is possible to construct an alloy of these elements which has the properties necessary for the future generation fuels.

In this work the Cu_3Pd (110) (1×2) surface is investigated. The aim of this study is to describe the surface with Embedded Atom Method (EAM) potential functions. The advantage of the EAM over other approaches for these calculations is two-fold. First, as described in paragraph 3.1., the embedding function that is used for pure metals should still be valid for the case of alloys. This makes the application of this method relatively simple. The other advantage of using EAM relates to the computational simplicity of the method that allows one to perform atomistic simulations. An overview of alloy and surface simulations performed with the EAM potentials is given in Daw *et al.* [2]. The agreement between experiments and theoretical predictions is good in case of segregation studies of Ni-Cu [3] and Au-Pd alloys. The method is also able to describe surface ordering effects in Cu-Au alloy-surfaces which agrees with symmetry and coverage found in experiments.

The Embedded Atom Method potentials are used in Monte Carlo simulations and free energy calculations. If it is feasible to describe the surface by EAM potentials, the method can be used to calculate properties of the surface, like the temperature dependent effects of the surface and phase transitions. Another interesting topic is the possibility to describe the composition of step edges on the surface. The composition of the step edges on the surface can be of considerable influence on the catalytic properties.

The results of the calculations will be compared with LEIS experiments on a

$Cu_{85}Pd_{15}$ (110) (1×2) surface carried out by Bergmans *et al.* [4][5]. These experiments are in agreement with earlier studies of this surface using angle resolved X-ray photo electron spectroscopy (ARXPS), temperature-programmed desorption (TPD) and low energy electron diffraction (LEED) [5]. These studies resulted in a proposed surface structure which consists of an almost complete copper top-layer and an ordered second layer of 50 at.% Cu and 50 at.% Pd.

This report is organized as follows. An overview of the CuPd alloy and the results of the LEIS experiments carried out by Bergmans are given in chapter 2. The embedded atom method and the simulation techniques are discussed in chapter 3. The Monte Carlo simulation technique is used to describe to surface properties. The Molecular dynamics simulation technique is discussed because it is used to simulate a TOF-SARS experiment. Chapter 4 covers a discussion of the results of the simulations and the free energy calculations. Chapter 5 deals with a conclusion and an outlook.

2. OVERVIEW CUPD

2.1. Bulk structure

The phase diagram of the CuPd alloys [6] is shown in fig. 1a. At low temperatures two regions exist in which the CuPd alloy orders. The α phase is based on the stoichiometric Cu_3Pd structure. The β phase is the stoichiometric CuPd structure. The Cu_3Pd structure

(a) CuPd phase diagram.

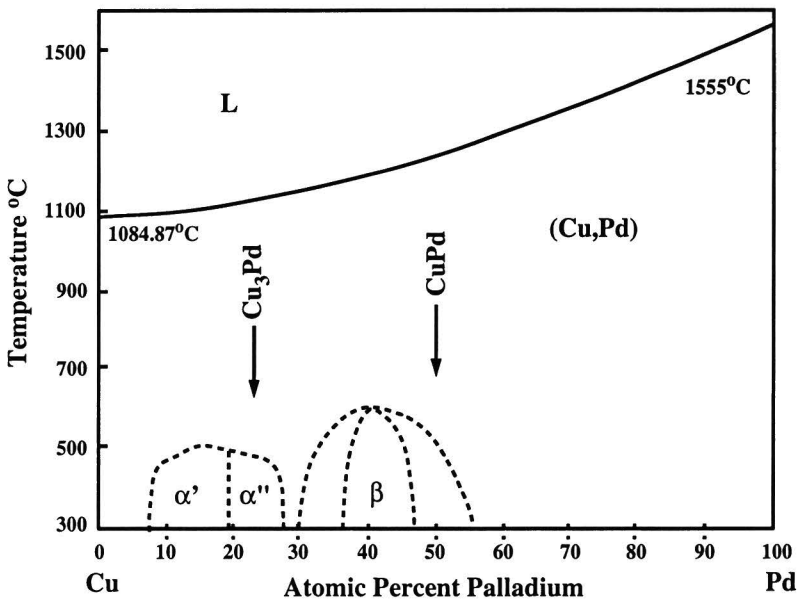

(b) Unit cell of a Cu_3Au ordered CuPd alloy.

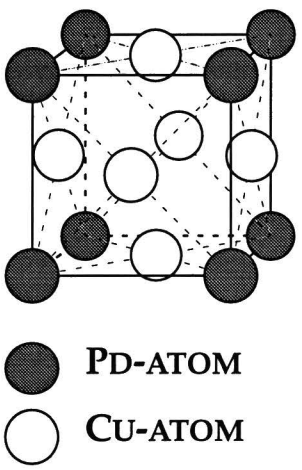

- Figure 1 - (a) Phase diagram of CuPd alloys. (b) Unit cell of the ordered Cu_3Pd structure.

has a Cu_3Au ($L1_2$) type of lattice. The unit cell of the stoichiometric Cu_3Pd structure is shown in fig. 1b. It is a Cu f.c.c. unit cell but with Pd atoms at every corner. The α phase in fig. 1a is divided in two regions, the α' and the α" phase. The α' structure has a cubic Cu_3Au unit cell. The unit cell of the α" structure is a Cu_3Au unit cell with a small distortion in one direction. This is called a tetragonal unit cell with an axial ratio of c/a=0.986 for a Pd percentage of ~24 at.% [6]. The disorder structure, indicated in fig. 1 as the (Cu,Pd) phase, is a perfect defined f.c.c. lattice with a random distribution of Cu and Pd atoms. The lattice spacings of the alloy as function of the composition are given in fig. 2. The lattice parameter of the ordered state is the same as that of the disordered state. The crystal with 15 at.% palladium shows an order-disorder transition at T~770K (fig. 1a). At a temperature of T~730K the order-disorder transition of $Cu_{75}Pd_{25}$ occurs.

In this work we mainly focus on the Cu_3Pd crystal with a (110) surface and where possible also on the $Cu_{85}Pd_{15}$ crystal. The bulk CuPd phase diagram indicates

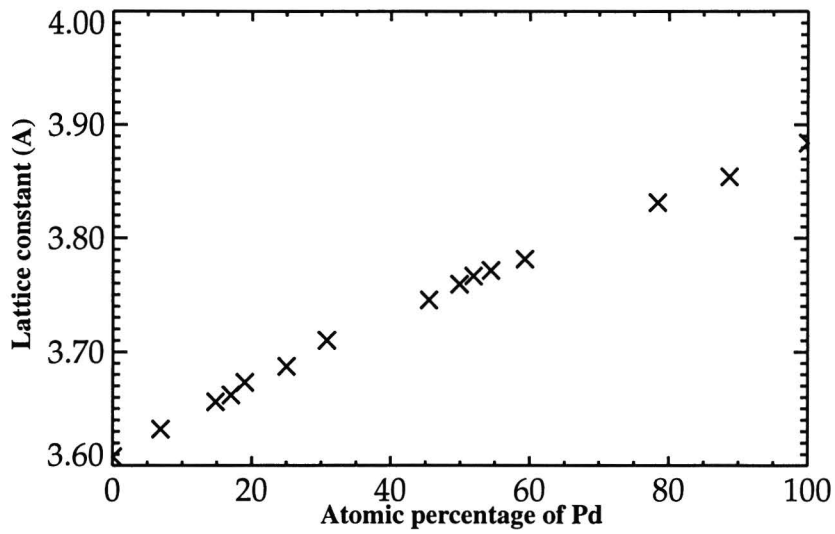

- Figure 2 - Lattice parameter as function of percentage Pd in alloy. These lattice spacing were reported to be accurate to ~0.05% [7].

that at a temperature below ~730K the Cu_3Pd bulk will have Cu_3Au order at this composition. A cut along the (110) plane will therefore give alternate layers of 50 at.% Cu and 50 at.% Pd or 100% Cu at the stoichiometric Cu_3Pd composition. So there are two possible terminations of the (110) surface in case of no reconstruction or segregation, one with 100% Cu in the first layer and 50 at.% Cu and 50 at.%Pd in the second layer. This surface is shown in fig. 3. The second possibility is a surface with 50 at.% Cu and 50 at.% Pd in

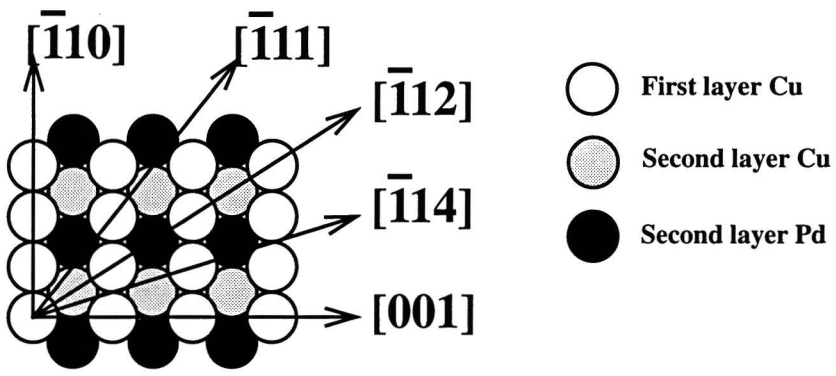

- Figure 3 - Proposed structure of the $Cu_{85}Pd_{15}$ (110) (2x1) surface (after Holmes et al. [3]) and of the Cu_3Pd (110) (2x1) surface.

the first layer and 100% Cu in the second layer. The layer with 50 at.% Cu and 50 at.% Pd is ordered for both options. Due to the ordering of Pd in the [110] direction, low energy electron diffraction (LEED) experiments of this surface will show a (2×1) pattern. A $Cu_{85}Pd_{15}$ crystal has Cu_3Au order below T~770K. The $Cu_{85}Pd_{15}(110)$ (2×1) surface investigated by Bergmans *et al.* [5] can therefore be used as comparison for the simulation results.

2.2. Previous experimental results

With ion scattering experiments the $Cu_{85}Pd_{15}(110)$ (2×1) crystal surface was investigated by Bergmans *et al.* [4][5]. The results of these experiments are important for the rest of this investigation and therefore the two ion scattering techniques and the results of the experiments will be discussed shortly. The techniques are implemented in an experimental setup as shown in fig. 4.

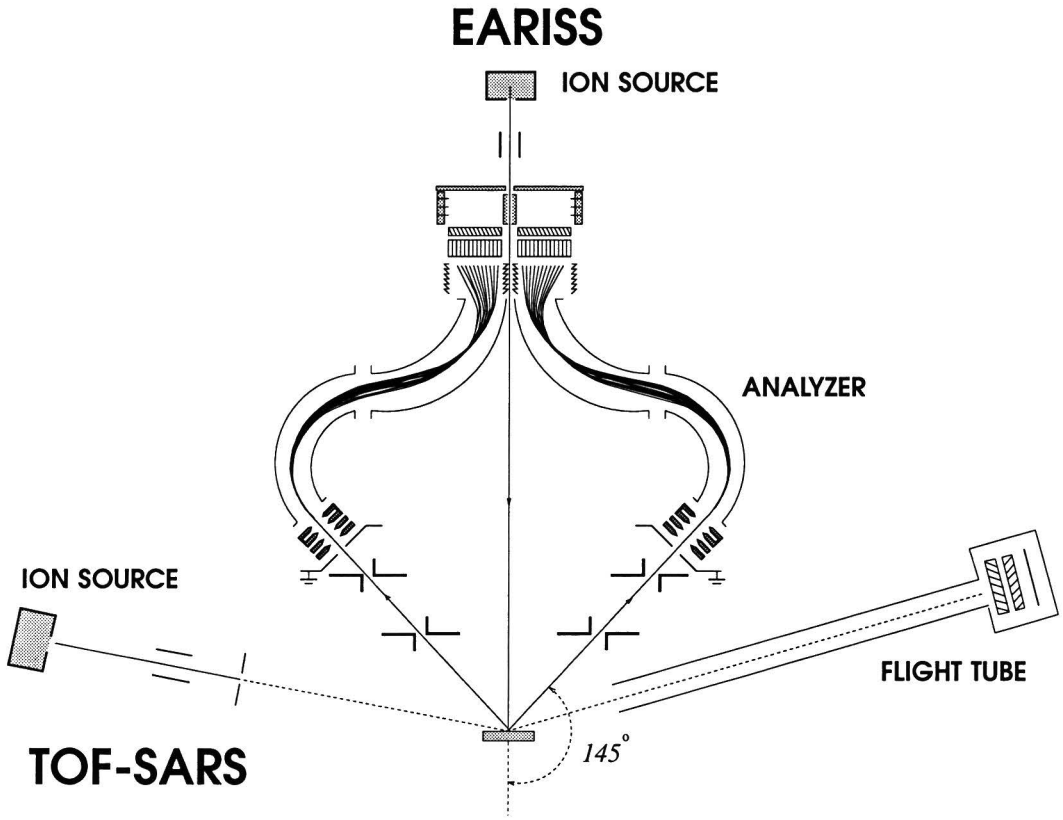

- Figure 4 - Schematic representation of the experimental setup used to investigate the $Cu_{85}Pd_{15}$-crystal by Bergmans et al. [5].

In both methods ions are accelerated to a kinetic energy of a few keV and directed towards the sample. An detector will registrate the scattered ions. Depending on the angle of incidence different processes can occur.

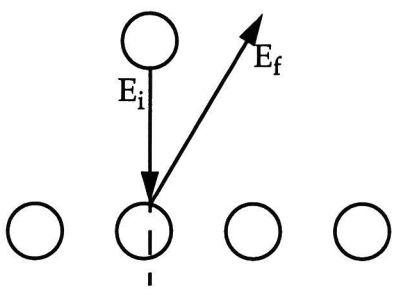

- Figure 5 - An ion with kinetic energy E_i impinges on the surface and is backscattering by the surface atoms. The backscattering ion will have a kinetic energy E_f. The EARISS is based on this process.

The energy and angle resolved ion scattering spectrometer (the EARISS) uses an angle of incidence of 90° with respect to the surface plane. The EARISS setup is shown in fig. 4. The ion source produces low energy ions and accelerates them towards the surface. A fraction of the incident ions is backscattered (fig. 5). Ions backscattered over an angle of 145° will be detected. The loss in energy and the azimuthal distribution of these backscattered ions can be used to determine the surface composition. The system is much more sensitive than other techniques because it detects simultaneously the energy and the azimuthal angle of the scattered ions.

The composition of the layers is determined using 2 keV Ne^+ ions. Because of the open structure of the (110) surface, both the first and second layer can be measured. The integration over the Pd-peak obtained with the EARISS as function of the azimuth is

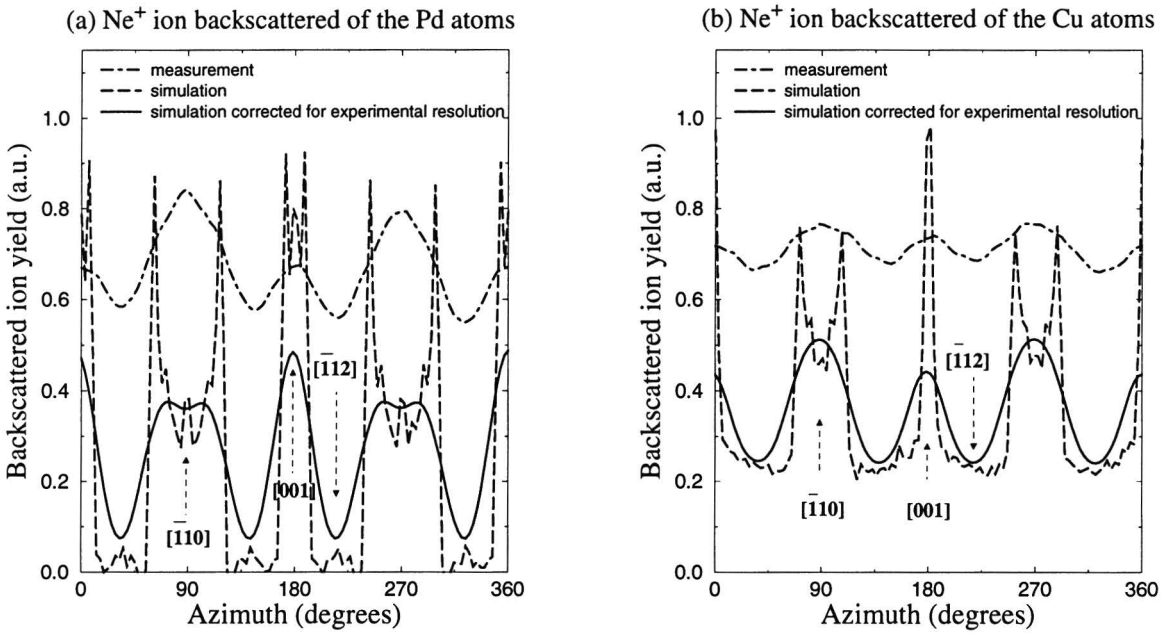

- Figure 6 - Azimuthal distribution of 2 keV Ne^+ ions backscattered off the surface atoms in the $Cu_{85}Pd_{15}$(110 surface as obtained with the EARISS. The simulations in the figure are performed by

shown in fig. 6a. Fig. 6b shows the same measurements for ions that have scattered of the Cu atoms. From fig. 6a it can be determined that palladium is present in the second layer because the intensity as function of the azimuth varies. These variations are the result of blocking of the ions scattered from the second layer in certain directions. In case of a $Cu_{50}Pd_{50}$ terminated first layer and a 100% copper containing second layer the intensity would be the same in all directions. Because the detector can only detect ions, the neutralization probability has to be considered. The ions scattered from the second layer spend a longer time at the surface and therefore will have a larger neutralization probability. The result is a much lower contribution to the signal from second layer atoms than the contribution of the first layer. Taking the neutralization probability and the resolution of the EARISS in account the composition of the surface was determined. For the

first layer a slight depletion in Pd is found (11 ± 2 at.%) whereas the second layer is strongly enriched in Pd (40 ± 8 at.%) .

The other technique used is time-of-flight forward scattering and recoil spectroscopy (TOF-SARS). The TOF-SARS measurements were performed using 1.5 keV Ar^+ ions with an incident angle of 13.6° with respect to the surface plane [5]. The detector has a fixed angle of 35° with respect to the ion source. A fraction of the ions will be scattered directly, called *single scattering* (fig. 7a). Some atoms will collide with two or more surface atoms before leaving the surface (fig. 7b). This collision is called *multiple scattering*. Some

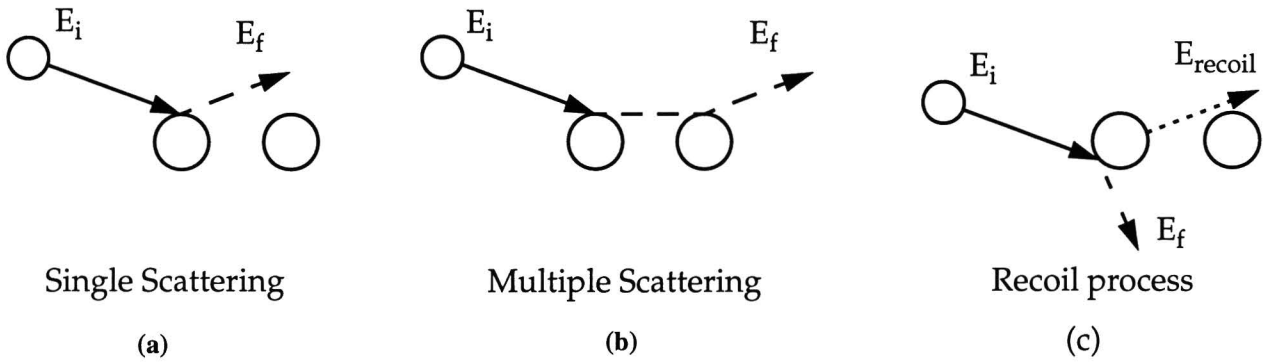

- Figure 7 - An ion with kinetic energy E_i collides with the surface atoms. After the collision the energy of the ion will be E_f. In the recoil process the recoiled surface atom will leave the surface with kinetic energy E_{recoil}.

surface atoms may get enough energy during the collision process to escape from the surface. These atoms are called *recoil atoms* (fig. 7c). The ions as well as the atoms scattered towards the detector will be detected and their flight time will be obtained. From this flight time the kinetic energy can be calculated.

(a) Time-of flight spectrum of $Cu_{85}Pd_{15}$ (110) obtained along the [-114] direction.

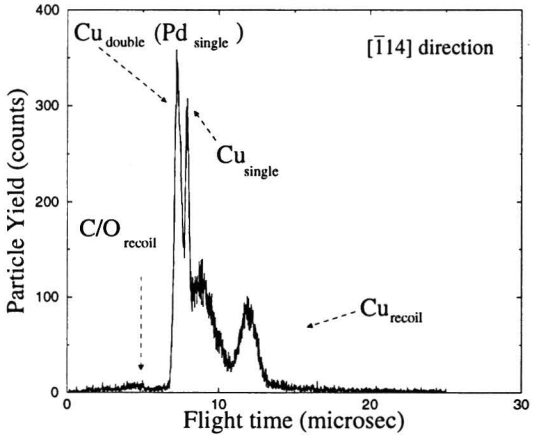

(b) Intensity of the Cu-recoil peak as a function of the azimuth of the $Cu_{85}Pd_{15}$ (110) surface.

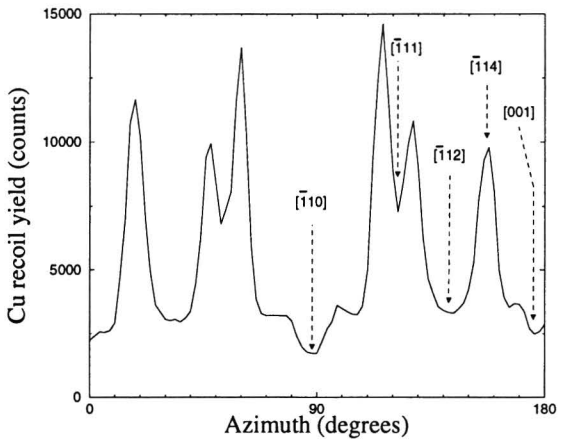

- Figure 8 - The data were obtained with TOF-SARS using 1.5 keV Ar^+ ions at an incident angle of 13.6° with respect to the surface plane, and a scattering angle of 35°.

The spectrum of the measurement in the [-114] direction is shown in fig. 8a. In this spectrum the dominant peaks are the Cu single collision, the Cu double collision and a Cu recoil peak. In the Cu double collision peak is also a contribution of the Pd single collision peak included. The fourth dominant peak, between the Cu recoil and Cu single collision peak, is not assigned. In fig. 8b, the intensity of the recoil peak versus azimuthal angle is plotted. From this spectrum we can determine that the (2×1) LEED pattern is not the result of a missing row structure. Consider for example the minimum in the [-112] direction. In case of a missing row structure the distance between the atoms in the [-112] direction would be optimum, and therefore a maximum in intensity would be expected instead of the observed minimum in the spectrum.

2.3. Why simulations?

The conclusion of the EARISS experiments is that the first layer is slightly depleted in Pd $(11 \pm 2$ at.%) The second layer is strongly enriched in Pd $(40 \pm 8$ at.%) assuming that the relative neutralization probability for the second layer is the same as for the first layer. These experimental result are in reasonable agreement with a proposed model for the $Cu_{85}Pd_{15}$ (110) (2×1) surface. At a certain temperature this (2×1) ordering will disappear.

The conclusion of the TOF-SARS experiments is that the surface is unreconstructed. The problem in these experiments is a large peak at ~9 microseconds in the spectrum. The origin of this peak is not clear.

The aim of this study is to describe the Cu_3Pd surface with Monte Carlo simulation and to obtain the surface ordering temperature. The Monte Carlo simulations can be used to calculate properties like composition and structure of steps on the surface or phase transition effects at the surface. Simulation of the surface behavior is particularly interesting because other techniques can only be used in case the composition and configuration is known.

Another interestic topic is the unexplained peak in the TOF-SARS spectrum. Molecular dynamics simulations are performed in order to investigate the origin of the different peaks in the TOF-SARS spectrum.

3. THEORY AND SIMULATION TECHNIQUES

In this chapter the simulation techniques are described. A Monte Carlo method is used to calculate the equilibrium surface and bulk structure of the CuPd alloys. The statistical mechanics and the technique used in the Monte Carlo simulation are discussed in section 3.2. The TOF-SARS experiments are simulated by Molecular dynamics simulation. The Molecular dynamics method will be discussed in paragraph 3.3. The interaction potentials used in the calculations will be discussed in the next paragraph.

3.1. The interaction potential

The interactions between the different atoms are described by many-body potentials, the so-called Embedded Atom Method (EAM) potentials described by Daw and Baskes [8]. It is a semi-empirical, many-atom potential for computing the total energy of a metallic system. This approach has been widely used to study a broad range of problems in metals and alloys like: phonons, liquid metals, defects, grain boundary structure, alloys, interdiffusion in alloys, fracture, surface structure, surface absorbate ordering, segregation to surface and grain boundaries, surface order-disorder transitions, surface ordered alloys and surface phonons [9].

The starting point of the embedded-atom method is the approximation of the total electron density at a given lattice site i by a superposition of the free atomic densities ρ_j^a of the remaining atoms j given by:

$$\rho_i = \sum_{j \neq i} \rho_j^a (|r_i - r_j|) \,. \tag{1}$$

In Eq.(1) it is also assumed that the atomic electron densities are spherical. The total energy takes the form:

$$E_{tot} = \sum_i F_i(\rho_i) + \frac{1}{2} \sum_{i \neq j} \Phi_{ij}(R_{ij}) \tag{2}$$

In this formula F_i is the energy to embed an atom i into the surrounding electron density. The second term is a sum over the pair interactions describing the short range nuclear repulsion. The EAM is particularly appealing for studies of alloys because the embedding energy F is independent of the source of the electron density. Therefore the same embedding energy can be used for an atom in an alloy that would be used in an pure metal.

The embedding function is uniquely defined using the universal scaling equation of Rose *et al.* [10] which shows that the total energy of most of the metals can be found as a function of lattice constant by:

$$E_{Rose}(a) = -E_{sub}(1 + a^*) e^{-a^*} \tag{3}$$

where a^* is a measure of deviation from equilibrium,

$$a^* = \left(\frac{a}{a_0} - 1\right)\sqrt{\frac{9B\Omega}{E_{sub}}} \tag{4}$$

The introduced bulk parameters are the equilibrium sublimation energy E_{sub}, the bulk modulus B, the equilibrium lattice constant a_0 and the equilibrium volume per atom Ω. Combining Eq. (2) and Eq. (3) the embedding function is

$$F(\rho_i) = E_{Rose}(a) - \frac{1}{2}\Phi_i(a) \tag{5}$$

To apply this method, the electron density and the pair repulsion should be determined. This can be done in two different ways: by theoretical considerations or by fitting to experimental data.

Table 1: Parameters defining the effective charges (Eq. (8)) and the atomic density (Eq. (6)) [11].

	Cu	Pd
Z_0	11	10
α	1.7227	1.2950
β	0.1609	0.0595
ν	2	1
n_s	1.000	0.8478

In this study the method developed by Foiles *et al.* is used [11]. The electron densities are computed from Hartree-Fock wave functions [12] by

$$\rho^a(R) = n_s\rho_s(R) + n_d\rho_d(R)\,, \tag{6}$$

with n_s and n_d are the number of outer s and d electrons and ρ_s and ρ_d are the densities associated with the s and d wave functions. The total number of s and d electrons, $n_s + n_d$, is fixed to be 10 for Pd and 11 for Cu. Thus the atomic density of each element depend on one parameter, n_s.

The pair interaction function is chosen as:

$$\Phi(R) = \frac{Z_A(R)\,Z_B(R)}{R} \tag{7}$$

where

$$Z(R) = Z_0(1 + \beta R^\nu)\,e^{-\alpha R} \tag{8}$$

The pair interaction term is purely repulsive. The value of Z_0 is the total number of outer electrons of the atom, thus $Z_0 = 10$ for Pd and $Z_0 = 11$ for Cu. Taking $\nu = 1$ for Pd and $\nu = 2$ for Cu leads to a good representation of the elastic constants as found empirically.

There still remain three adjustable parameters α, β and n_s needed to determine the embedding energy. The values of α and β are primarily determined by the shear moduli of the pure metals and the vacancy-formation energy. The parameter n_s will be determined so that the potential will give the proper heats of solution of the alloys. The parameters derived by Foiles *et al.* [11] to define the electron density and the pair interactions are given in Table 1.

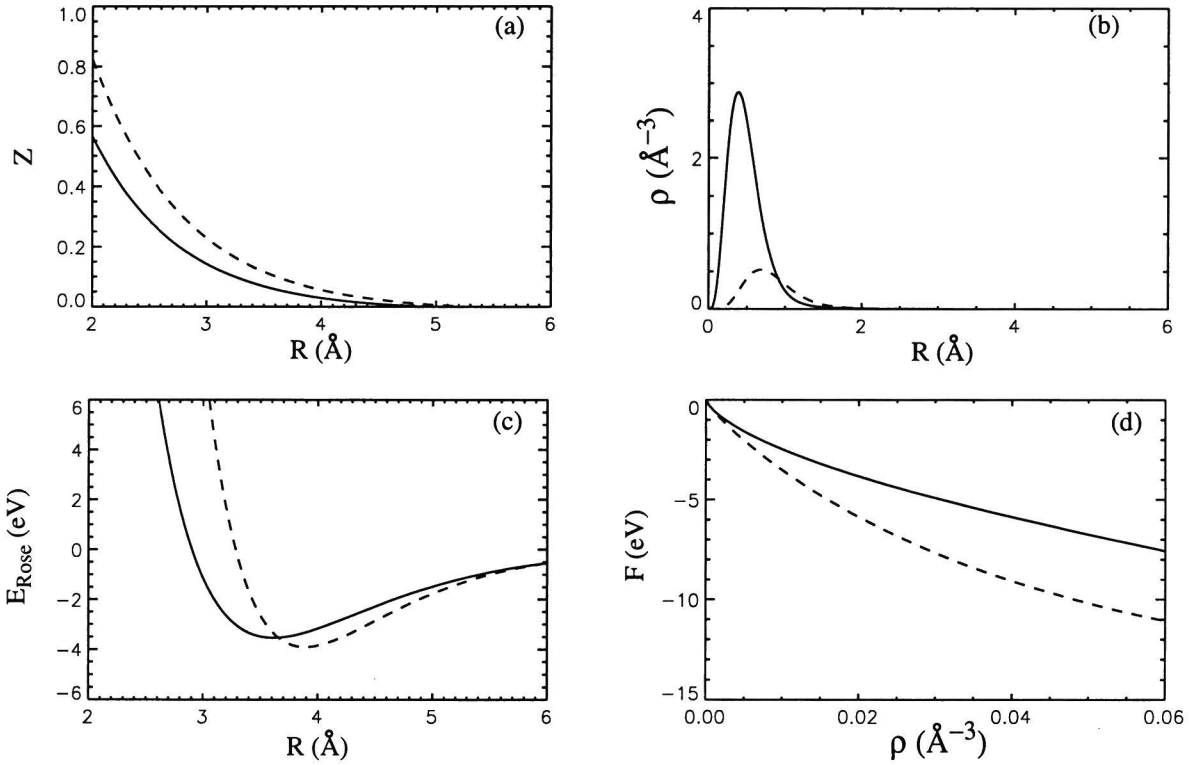

- Figure 9 - (a) The effective charge Z(R) used to define the pair interaction. (b) Electron density distribution ρ(R). (c) Universal scaling equation of Rose. (d) Embedding energy F(r). The solid curves show copper and the dashed lines show palladium.

3.2. Monte Carlo simulation

Monte Carlo simulation is a well established approach to model a wide variety of equilibrium thermodynamic phenomena at finite temperatures [14]. The underlying concept is that a system which is not in equilibrium is allowed to evolve towards equilibrium through a serie of configurational changes. Monte Carlo stands for using a random number generator to decide whether or not such a configurational change will be accepted.

3.2.1. Monte Carlo simulation technique

In the Monte Carlo simulation a calculation is made of thermodynamic average of a certain property. The thermodynamic average of a certain property A is given by

$$\langle A \rangle = \frac{\int \exp(-\beta K(p))\, dp \int A(q) \exp(-\beta U(q))\, dq}{\int \exp(-\beta K(p))\, dp \int \exp(-\beta U(q))\, dq}, \tag{9}$$

as an integral over momentum (p) and configurational space (q) where $\beta = 1/kT$. The momentum and configurational space together is called the phase space. The basic idea of the Monte Carlo method is to calculate the phase space integral numerically. An integral $\int f(x)\, dx$ is approximated by a sum with a finite number of terms $\sum f(x)\, \Delta x$. Monte Carlo integration is used here because standard numerical integration routines take more calculation time before a reliable result is obtained.

The Monte Carlo method introduced here is the Metropolis method [15]. This is a sampling algoritm based on the idea of 'importance sampling'. Here the phase points are selected according to a probability P(p,q). The integral is taken over a simulation cell constructed of atoms on perfect lattice points. During the simulation the simulation cell will be allowed to make configurational changes. There are three different kinds of configurational variations included in the simulation:

i) An atom is chosen at random and the type of the atom will be changed with a certain probability. The desired bulk composition is obtained by adjusting the relative chemical potentials of the elements in the bulk. In general, a prescribed set of chemical potential differences will define the equilibrium composition of the system at a given temperature.

ii) The position of the atoms may change in small displacements from their current position. This simulates atomic vibrations and relaxation effects between atoms of different elements.

iii) The entire volume can be expanded or compressed. The volume of a crystal is changed by scaling simultaneous all the coordinates of all the atomic positions. This variation includes the thermal expansion effects.

A change in configuration is accepted or rejected depending on the thermodynamic probability of the occurrence. Repeating this procedure many times will usually lead to thermodynamic equilibrium. The transition probability can be calculated using statistical mechanics.

3.2.2. Statistical Mechanics

Transition probability

The Hamiltonian of the simulation cell can be expressed as a sum of kinetic and potential energy functions of the set of coordinates q_i and momenta p_i of each atom i:

$$H(\mathrm{p,q}) = K(\mathrm{p}) + U(\mathrm{q}) \tag{10}$$

with kinetic energy:

$$K(\mathrm{p}) = \sum_{i=1}^{N} \frac{\mathrm{p}_i^2}{2m_i} \tag{11}$$

If N, the number of atoms in the simulation cell, is large enough the concept of a continuous density of phase points can be introduced. To do this, we define a function $\rho_{p,q}(p_1, p_2,\ldots, p_{3N}, q_1, q_2,\ldots, q_{3N}; t)$ so that $\rho_{p,q}(p, q; t)dp\,dq$ is the number of the phase points, at time t, in the element of volume $dp_1, dp_2,\ldots, dp_{3N}, dq_1, dq_2,\ldots, dq_{3N}$ of phase space. This density can be normalized in such a way that it becomes the probability density of the state (p, q).

Using Liouville's theorem [16][17], for the probability density of the state (p,q) of a canonical system (constant N, T, V) it can be found that:

$$\rho_{p,q} = C \times \exp\left(-\beta H(\mathrm{p,q})\right) \tag{12}$$

Then the probability density can be described by:

$$p_{p,q} = \frac{\exp\left(-\beta H(\mathrm{p,q})\right)}{Q} \tag{13}$$

with

$$Q = \frac{1}{N!}\frac{1}{h^{3N}}\int\int \exp\left(-\beta H(\mathrm{p,q})\right) dp\,dq \tag{14}$$

where a constant h is introduced in order to make Q dimensionless. Q is called the *partition function.*The N! is included because of the indistinguishability of the particles, in accordance with the rule of 'correct Boltzmann counting'.

Because the energy is expressible as a sum of kinetic and potential energy contributions the probability for a certain configuration is:

$$p_q = \frac{\exp\left(-\beta U(\mathrm{q})\right)\int \exp\left(-\beta K(\mathrm{p})\right) dp}{Q} = \frac{1}{\Lambda^{3N}}\frac{\exp\left(-\beta U(\mathrm{q})\right)}{Q} \tag{15}$$

Λ being the thermal de Broglie wavelength

$$\Lambda = \left(\frac{h^2}{2\pi m k_B T}\right)^{\frac{1}{2}}. \tag{16}$$

For a system with a fixed pressure P instead of a fixed volume V, the so called isothermal-isobaric ensemble, the probability density is proportional to

$$p_{p,q,V} \sim \exp\left(-\beta\left(H(\mathrm{p,q}) + PV\right)\right). \tag{17}$$

In this case in the partition function is also a sum over V is included.

Another system that will be considered is one with a variable number of particles. In this case the chemical potential μ will be kept fixed. The probability density of this ensemble, the grand-canconical ensemble, will be proportional to

$$p_{p,q,N} \sim \exp\left(-\beta\left(H(\mathrm{p,q}) - \mu N\right)\right). \tag{18}$$

In the partition function of this ensemble a sum over N is included.

In the simulations a thermodynamic system is used which is a lattice with N_1 atoms of component 1 and N_2 atoms of component 2. N_1 and N_2 are variable but the total number of atoms $N=N_1+N_2$ is fixed. The other fixed parameters are temperature (T), pressure (P) and the chemical potentials μ_1, μ_2 of the two particle types. In a Monte Carlo simulation this system is allowed to make two different configurational changes. Configurational changes with constant μ_1, μ_2, V and T, described by the grand-canonical ensemble and configurational changes with constant N, T and P, described by an isothermal-isobaric ensemble.

In the configurational change with constant μ_1, μ_2, V and T, an atom is chosen at random and it is displaced by a certain amount, less or equal to 0.1 nm. The type of this atom will be changed with a certain probability[1]. With the statistical mechanics the transition probability for this Monte Carlo step is calculated. The probability that the ensemble will have the parameters of the system before a change is made is:

$$p_{initial} = \frac{1}{\Lambda_1^{N_1}\Lambda_2^{N_2}} \frac{\exp\left(\beta\left(\mu_1 N_1 + \mu_2 N_2\right)\right)\exp\left(-\beta E_{initial}\right)}{Q_{\mu_1\mu_2 VT}} \tag{19}$$

with $N_2 = N - N_1$. The probability that the ensemble will have the parameters of the system after the change is made is

$$p_{final} = \frac{1}{\Lambda_1^{N_1+1}\Lambda_2^{N_2-1}} \frac{\exp\left(\beta\left(\mu_1\left(N_1+1\right) + \mu_2\left(N_2-1\right)\right)\right)\exp\left(-\beta E_{final}\right)}{Q_{\mu_1\mu_2 VT}} \tag{20}$$

Therefore the probability that the system will change is

1. There are four possible interchanges of atomic types. They are as follow for the CuPd alloy: (a) Pd for Cu; (b) Cu for Pd; (c) Pd for Pd; (d) Cu for Cu. Replacements (c) and (d) do not produce a change in local compositions; they may, however, result in displacements.

$$\frac{p_{final}}{p_{initial}} = \frac{\Lambda_2}{\Lambda_1}\exp\left(-\beta\left(\Delta E - \Delta\mu\right)\right) \tag{21}$$

with $\Delta\mu = \mu_1 - \mu_2$ and $\Delta E = E_{final} - E_{initial}$.

In the other configurational change the volume of the simulation is changed. The pressure P, the number of particles N and the temperature T will be kept constant during this process. The probability of this ensemble can be given by

$$p_{initial} = \frac{V^N{}_{initial}}{\Lambda_1^{N_1}\Lambda_2^{N_2}}\frac{\exp\left(-\beta P V_{initial}\right)\exp\left(-\beta E_{initial}\right)}{Q_{NpT}} \tag{22}$$

In the probability of this system an extra factor V^N has to be included because Monte Carlo simulation is integrating over a unit cell while the integral has to be calculated over the volume V. The probability density of the system after the Monte Carlo step is given by

$$p_{final} = \frac{V^N{}_{final}}{\Lambda_1^{N_1}\Lambda_2^{N_2}}\frac{\exp\left(-\beta P V_{final}\right)\exp\left(-\beta E_{final}\right)}{Q_{NpT}} \tag{23}$$

Therefore the probability of transition is

$$\frac{p_{final}}{p_{initial}} = \left(\frac{V_{final}}{V_{initial}}\right)^N \exp\left(-\beta P\left(V_{final} - V_{initial}\right)\right)\exp\left(-\beta\left(E_{final} - E_{initial}\right)\right) \tag{24}$$

Chemical Potential

The chemical potential is used in the simulations to control the composition of the alloy. The chemical potentials measure how the Gibbs free energy of a phase depends on any changes in its composition. In random alloys the chemical potential difference between the elements is found by adjusting the chemical potential difference until the desired bulk composition is obtained. In case of an ordered alloy the chemical potential has to be calculated exactly. In Cu_3Pd this can be done easily because all the Cu atoms have the same neighbor atoms and all Pd atoms have the same neighbor atoms. We follow the method of Foiles et al. [18].

Consider a system with N lattice sites that are divided into two sublattices, one with A atoms and the other one with atoms of type B. In the A_3B alloy there will be three A sites for each B site. Each site will be occupied by a type A atom or a type B atom. For the energy per atom of this system we can write:

$$\frac{E}{N} = \frac{E_0}{N} + n_{AB}E_{AB} + n_{BA}E_{BA} \tag{25}$$

where E_0 is the energy of the ideal lattice, n_{AB} is the number of B atoms on an A lattice

site and E_{AB} is the energy difference between a lattice with one A lattice site occupied by a B atom and the ideal lattice. The configurational entropy per atom of the system is

$$\frac{S}{N} = \frac{3}{4}s\left(\frac{4}{3}n_{AB}\right) + \frac{1}{4}s\left(4n_{BA}\right) \tag{26}$$

with the entropy s given by

$$s(x) = -k_B\left[x\ln(x) + (1-x)\ln(1-x)\right] \tag{27}$$

The total number of type A atoms will be

$$N_A = N\left(\frac{3}{4} + n_{BA} - n_{AB}\right) \tag{28}$$

and the number of type B atoms

$$N_B = N\left(\frac{1}{4} + n_{AB} - n_{BA}\right) \tag{29}$$

Minimization of the grand potential $E - TS - \sum\mu_i N_i$ gives for the number of B atoms on the A lattice

$$n_{AB} = \frac{3}{4}\left(\frac{\exp\left(-\frac{(E_{AB}+\mu_A-\mu_B)}{k_BT}\right)}{1+\exp\left(-\frac{(E_{AB}+\mu_A-\mu_B)}{k_BT}\right)}\right) \tag{30}$$

and for the A atoms on the B lattice

$$n_{BA} = \frac{1}{4}\left(\frac{\exp\left(-\frac{(E_{BA}+\mu_B-\mu_A)}{k_BT}\right)}{1+\exp\left(-\frac{(E_{BA}+\mu_B-\mu_A)}{k_BT}\right)}\right) \tag{31}$$

In an ideal composition the number of B atoms on the A lattice will be equal to the number of A atoms on the B lattice (n_{AB}=n_{BA}). Taking the zero temperature limit gives:

$$\mu_A - \mu_B = \frac{(E_{BA} - E_{AB})}{2} \tag{32}$$

With the Gibbs free energy equation

$$G = H - TS = U + PV - TS \tag{33}$$

and the relation between the Gibbs free energy and the chemical potential

$$G = \sum_i n_i\mu_i \tag{34}$$

we find for zero pressure

$$\mu_A N_A + \mu_B N_B = E - TS \tag{35}$$

One of the chemical potentials can be eliminated by combining Eq. (32) and Eq. (35). In the zero temperature limit this gives

$$\mu_A = \frac{E_0}{N} + \frac{(E_{BA} - E_{AB})}{8} \tag{36}$$

3.3. Molecular dynamics simulation

The Molecular dynamics simulation discussed here will be used to describe the interaction process between a particle with a certain kinetic energy and a sample. Molecular dynamics treats a group of atoms as classical particles. The interaction between the atoms is described by a potential energy function. From this function, the forces on the atoms are calculated, which in turn gives the positions and velocity by solving the Newton's equation of motion. The potential functions used here are the embedded atom potentials. To incorporate more repulsive interactions at small internuclear separations, the potentials are splined to a Moliere potential with a screening length of 0.83 times the Firsov value [19].

4. RESULTS

With the methods discussed in chapter 3 the bulk and the surface structure of a Cu_3Pd and where possible for a $Cu_{85}Pd_{15}$ crystal are calculated using the EAM potentials. The Cu_3Pd structure is used here instead of a $Cu_{85}Pd_{15}$ because some parameters like for instance the chemical potential can only be calculated for perfectly ordered structures, where all the chemical identical atoms have the same neighbor atoms. Because the $Cu_{85}Pd_{15}$ as well as the Cu_3Pd structure show Cu_3Au order, the results of the $Cu_{85}Pd_{15}(110)$ (2×1) experiments by Bergmans *et al.* [4][5] will be compared to the results of the Cu_3Pd (110) surface simulations. The potential functions were taken from Foiles *et al.* [11]. They constructed a set of potentials for Cu, Ag, Au, Ni, Pd, Pt, and their alloys.

The surface energies for a Cu, a Pd and a Cu_3Pd crystal is calculated at a temperature of 0K using the EAM potentials. The values will be compared to values known from literature. Monte Carlo simulations are performed to describe the properties of the surface at finite temperatures. Molecular dynamics simulations are carried out to simulate the TOF-SARS experiments and to assign the peaks in the TOF-SARS spectrum.

4.1. Free energy calculation of the bulk structure

For a temperature of T=0K the Gibbs free energy of the Cu_3Pd and the $Cu_{85}Pd_{15}$ crystal bulk is calculated. The Gibbs free energy is calculated using Eq. (33) for a crystal with 864 atoms. The crystal structure in thermodynamic equilibrium has the lowest Gibbs free energy possible for the composition.

The Gibbs free energy of the ordered Cu_3Pd crystal is G = -3.71235eV/atom. The disordered crystal consists of randomly distributed Cu and Pd atoms on a perfect f.c.c. lattice. The average Gibbs free energy of ten configurations of the disordered Cu_3Pd crystal is G = -3.675±0.001 eV/atom. The ordered Cu_3Pd structure has the lowest Gibbs free energy at a temperature of T~0K and will therefore be the equilibrium structure.

For the composition $Cu_{85}Pd_{15}$ the ordered crystal is a perfectly ordered Cu_3Pd-crystal with randomly Pd atoms interchanged for Cu atoms to obtain the correct composition. The average Gibbs free energy of ten ordered crystal configurations is G = -3.63729 ±0.00002 eV/atom. An average value has to be calculated because the $Cu_{85}Pd_{15}$ crystal still shows a certain amount of disorder. The disordered $Cu_{85}Pd_{15}$ crystal has a f.c.c. lattice with a random distribution of Cu and Pd atoms. The average Gibbs free energy of ten disordered $Cu_{85}Pd_{15}$ crystal configurations is G = -3.623±0.001 eV/atom. The ordered $Cu_{85}Pd_{15}$ structure has the lowest Gibbs free energy and is therefore the equilibrium structure at a temperature of T~0K.

The Gibbs free energy can be calculated as a function of the temperature in the harmonic approximation. In the harmonic approximation, a quadratic expansion is made about the equilibrium positions. The vibrational modes and frequencies of the lat-

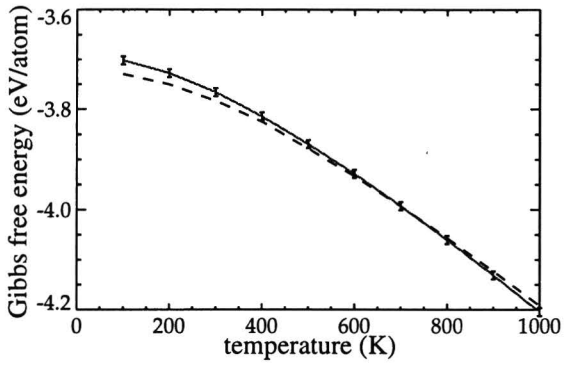

- Figure 10 - Gibbs free energy as function of the temperature of a Cu_3Pd crystal. The dashed line is the Gibbs free energy of the ordered Cu_3Pd crystal. The solid line is the average Gibbs free energy of the disordered crystal.

tice are computed by diagonalizing the dynamical matrix as described in references [20] and [21] and the Gibbs free energy is computed as a sum over the vibrational modes. The Gibbs free energy of a random configuration includes also a configurational entropy term.

The Gibbs free energy for an ordered and a disordered Cu_3Pd crystal of 32 atoms is calculated and plotted as a function of temperature in fig. 10. The dashed line in the figure is the Gibbs free energy of the ordered Cu_3Pd crystal. The solid line is the average Gibbs free energy of ten disordered crystal configurations. The two lines cross at a temperature of T~700K. Below a temperature of T~700K the ordered Cu_3Pd structure will be the equilibrium structure. Above a temperature of T~700K the disordered Cu_3Pd structure will be the equilibrium structure.

The order-disorder transition temperature is very sensitive for a shift in the Gibbs free energy curves, as can be observed in fig. 10. Therefore, we would expect the transition temperature to be sensitive to the size of the unit cell.

4.2. Investigation of the bulk structure by Monte Carlo simulation

To investigate the influence of the temperature on the structure of the crystals accurately, Monte Carlo simulations have been done. In the Monte Carlo simulations the initial simulation cell contains 864 atoms on ideal lattice positions. Three dimensional periodic boundary conditions are employed to minimize size effects. In the bulk simulations the first configurational step as described in paragraph 3.2.1. is different. The number of atoms of each element is fixed during the simulation. Instead of taking one atom at random two atoms will be chosen and exchanged. The transition probability for this transition is

$$P(i \rightarrow f) = \frac{p_f}{p_i} = \exp(-\beta \Delta E) \tag{37}$$

The advantage of this method is that there is no need to know the chemical potential dif-

ference of the two elements. The volume is changed after approximately all the atoms of the simulation cell have undergone one Monte Carlo step. The transition probability for this step is given by Eq. (24) on page 15.

Whether or not a equilibrium state is achieved is judged by monitoring the evolution of different physical parameters as a function of the number of the Monte Carlo steps. In the case that the simulation cell has an ordered structure, this physical parameter will be the structure factor. In other cases the parameter will be the volume or the energy of the simulation cell.

The lattice constant as function of the composition is calculated. The initial simulation cell is a perfect fcc lattice with a random distribution of Cu and Pd atoms over the lattice sites, a disordered lattice. Because the lattice constant of the random states is equal to the lattice constant of the ordered states at the same composition [7], the lattice parameter can be compared directly to literature. In case of a 100% Cu or a 100% Pd crystal the lattice parameter calculated in the simulation matches perfectly with the values in literature. This is obvious because the potential functions are fitted to these parameters. Good agreement is obtained between the lattice parameters in literature and the lattice parameters calculated for the alloy as shown in fig. 11.

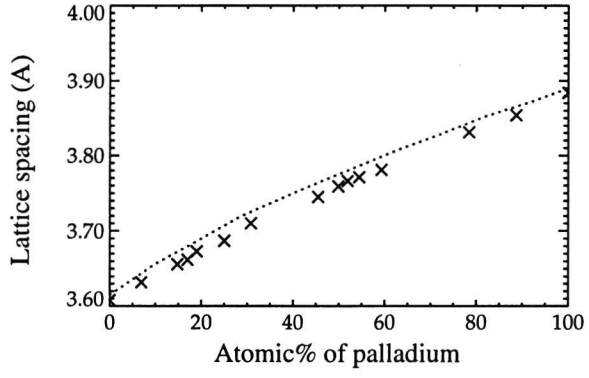

- Figure 11 - Lattice spacing as function of the atomic percentage of palladium in a CuPd alloy. The dashed line show simulation results, the crosses show the literature values [7].

In the literature it is reported that the $Cu_{85}Pd_{15}$ and the Cu_3Pd crystal will be ordered below a certain temperature T_{order} . This order temperature is 770K for the $Cu_{85}Pd_{15}$-crystal and 730K for the Cu_3Pd-crystal. To evaluate the ordering as a function of temperature in the simulation we calculate the structure factor, which will be used here as an order parameter. The structure factor is defined by

$$S_k = \frac{1}{N}\left\langle \left| \sum_i \exp\left((i)\left(\vec{k} \cdot \vec{R}_i \right) \right) \right|^2 \right\rangle \tag{38}$$

where the sum is over the Cu and Pd atoms, k is the wave vector in reciprocal space, R_i is the position of atom i and the angular brackets denote an average over the configurations generated in the simulations. The Cu_3Au structure will show peaks for k = (1,0,0),

(1,1,0), (2,1,0) and (2,1,1) in the structure factor [22]. These peaks will disappear in the disordered state.

4.2.1. Cu_3Pd

The initial simulation cell of the Cu_3Pd crystal is a perfect stoichiometric Cu_3Pd lattice. It is not possible to start with a disordered alloy because the simulation will not evolve to the stoichiometric Cu_3Pd structure. The simulation will probably be stuck in a local minimum before the ordered equilibrium is reached. Calculating the structure factor as function of temperature results in an order temperature of ~250K for the Cu_3Pd-crystal as shown in fig. 12. The structure factor shows a small decrease between 0K and ~200K. This reduction is the result of the increasing temperature because the atoms will get small displacements from their initial position for increasing temperatures. Between the 200-280K temperature trajectory the amount of order decreases resulting in a completely disordered bulk at temperatures above 280K.

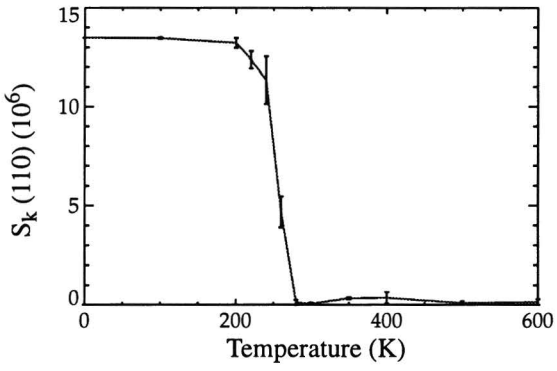

- Figure 12 - Structure factor with k = (110) as function of temperature. The simulated crystal is Cu_3Pd. For the simulation at the transition temperature 3 millions MC steps have been carried out before the structure factor converged.

4.2.2. $Cu_{85}Pd_{15}$

The initial simulation cell for the $Cu_{85}Pd_{15}$ simulation is a perfectly ordered Cu_3Pd-crystal with randomly Pd atoms interchanged for Cu atoms to obtain the necessary composition. It is not possible to start with a purely disordered alloy with 15% palladium and 85% copper because the simulation will not converge to an ordered alloy as before. The results of the simulation are shown in fig. 13. Above a temperature of 200K the stoichiometric structure is disappeared. The crystal will be completely random. For a temperature of 100K the crystal shows a structure factor of $\sim 3 \times 10^6$ after 10^7 Monte Carlo steps. Considering the monotonic decrease of the structure factor in time we can conclude that the order in the crystal at a temperature of 100K may disappear as well. For temperatures below 100K the monotonic decrease of the structure factor in time is smaller, but still existent. From the Gibbs free energy calculation at T~0K in paragraph 4.1 can be concluded that the crystal shows order at this temperature which implies that there is an

order-disorder transition temperature. The simulations are too much time consuming to obtain the exact order-disorder transition temperature.

(a) Structure factor as a function of temperature

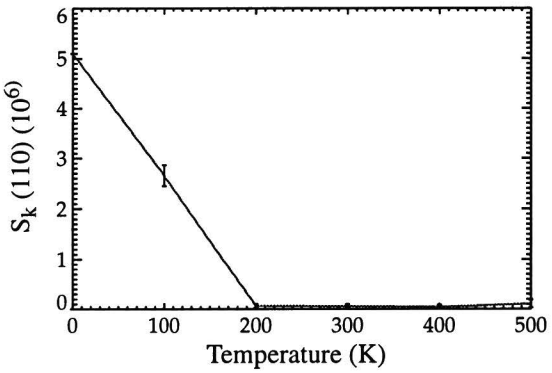

(b) Structure factor as a function of the number of Monte Carlo steps.

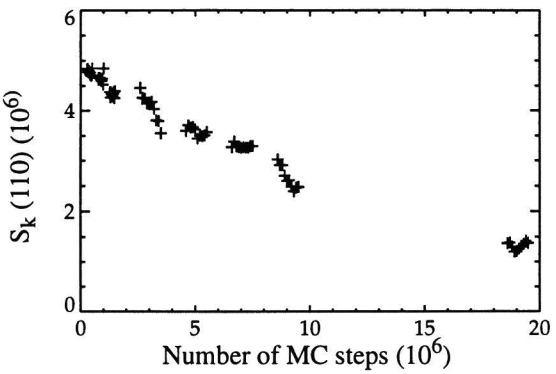

- Figure 13 - The k =(110) structure factor in case of $Cu_{85}Pd_{15}$ crystal simulations

4.3. Surface energy calculation of the crystal surfaces

The surface energy of the Cu_3Pd crystal is calculated at a temperature of T ~ 0K. A cut along the (110) direction will offer two possibilities of surface terminations. A surface with 100% Cu in the outermost layer and a ordered mix of Cu and Pd in the second layer. This surface termination is shown in fig. 14a. The other possibility is a $Cu_{50}Pd_{50}$ terminated surface with 100% Cu in the second layer as shown in fig. 14b.

(a) Cu terminated Cu_3Pd surface

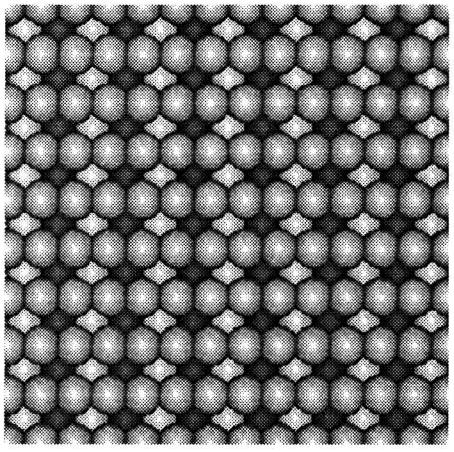

(b) $Cu_{50}Pd_{50}$ terminated Cu_3Pd surface

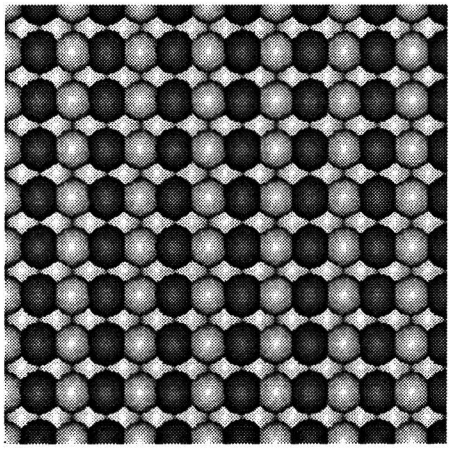

- Figure 14 - Initial surfaces of the Cu_3Pd simulation cell. The dark atoms are palladium atoms. The other atoms are copper atoms.

If μ_{Cu} and μ_{Pd} are the Cu and Pd chemical potentials, respectively, the surface energy per unit area γ is calculated with the relation [23]

$$A\gamma = E - \mu_{Cu} n_{Cu} - \mu_{Pd} n_{Pd} \tag{39}$$

Here E is the energy of the slab (which contains n_{Cu} copper and n_{Pd} palladium atoms) and A is the total surface area. The surface energy is calculated using a slab of 25 layers consisting of 16 atoms each. In order to perform the surface energy calculation of pure copper and pure palladium the chemical potentials of pure Cu and pure Pd have to be known. The chemical potential of pure materials can be calculated by dividing the bulk free energy by the total number of atoms. The chemical potential for pure Cu is $\mu_{Cu} = -3.540eV$ and for pure Pd $\mu_{Pd} = -3.910eV$. With Eq. (32) and Eq. (36) the chemical potentials of Cu and Pd are calculated for the Cu_3Pd structure at a temperature of 0 K. In the Cu_3Pd crystal the chemical potential of copper is $\mu_{Cu} = -3.565eV$ and palladium gives $\mu_{Pd} = -4.155eV$. The surface energy of the different surface terminations is shown in table 2. The surface energy is calculated for a surface with the atoms on ideal

Table 2: Surface energy of Cu, Pd and two Cu_3Pd surfaces.

Bulk structure	Surface structure	$\gamma_{initial}$ (J/m^2)	γ_{relax} (J/m^2)	γ_{lit} (J/m^2) [24]
Copper (fcc)	Cu [110]	1.42	1.41	1.85
Palladium (fcc)	Pd [110]	1.56	1.48	2.10
Cu_3Pd	Cu_{100} [110]	1.47	1.41	
Cu_3Pd	$Cu_{50}Pd_{50}$ [110]	1.41	1.36	

lattice positions ($\gamma_{initial}$) and for a surface where the atoms in the outermost two layers were free to relax (γ_{relax}). The surface energy of the Cu and the Pd crystal can be compared to the experimental values reported in literature (γ_{lit}) [24]. The $Cu_{50}Pd_{50}$ terminated surface has the lowest surface energy, and is therefore the preferred structure of the Cu_3Pd crystal.

4.4. Investigation of the crystal surfaces by Monte Carlo simulation

The properties of the Cu_3Pd surface for higher temperatures are simulated with Monte Carlo simulations. The initial simulation cell for the surface simulations is a perfect ordered Cu_3Pd-crystal and contains 3360 atoms. The number of layers in the simulation cell is 24 and each layer contains 140 atoms. The initial cell has two (110) surfaces, one 100% Cu terminated surface with a $Cu_{50}Pd_{50}$ composition in the second layer (fig. 14a) and a $Cu_{50}Pd_{50}$ terminated surface with 100% Cu in the second layer (fig. 14b). Periodic boundaries in the directions parallel to these surfaces are applied in order to minimize size effects.

In the surface simulations the chemical potential difference between the two elements is used to control the composition. Using the chemical potential, the grand-canonical approach, is similar with connecting the simulation cell to an infinite Cu_3Pd reservoir. With Eq. (32) and Eq. (36) the chemical potential of Cu is found to be $\mu_{Cu} = -3.565eV$ and the chemical potential of palladium gives $\mu_{Pd} = -4.155eV$ in the Cu_3Pd bulk at a temperature of 0 K.

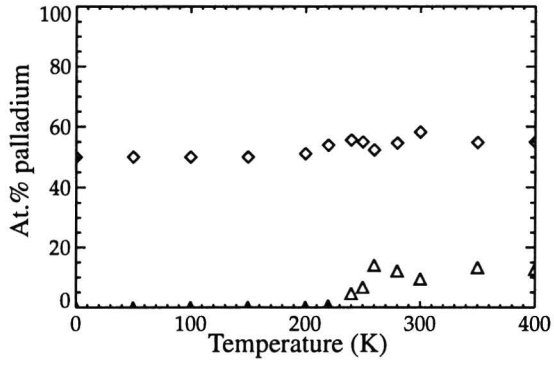

- Figure 15 - Palladium concentration in surface layers as function of the temperature (K). Diamonds: at.% Pd in outermost layer and triangles: at.% Pd in the second layer.

The simulation is in equilibrium after 4 million steps. The outermost layer of the surface with initially the 100% Cu terminated surface is enriched with Pd until a Pd concentration of 50 at.% is obtained. The second layer of this configuration will be enriched with copper. After 4 million Monte Carlo steps the copper concentration in the second layer will be ~100%.

The surface with initially a $Cu_{50}Pd_{50}$ structure (fig. 14b) is more stable during the simulation. Below a temperature of ~240K the surface will keep the same composition. In fig. 15 the composition of the first and the second layer of the initially $Cu_{50}Pd_{50}$ terminated surface is plotted as a function of the temperature. Initially the outermost layer consists of 50 at.% Cu and 50at.% Pd. This composition holds on in the calculated temperature range. The second layer of this configuration consists of 100% Cu atoms initially. Above a temperature of ~240K the second layer gets a small enrichment of palladium atoms in equilibrium.

The structure factor of the $Cu_{50}Pd_{50}$ terminated surface is calculated with Eq. (38). The sum in this equation is over the palladium atoms. The structure factor is plotted as function of k in fig. 16 for a temperature of 0K, 220K and 400K. Increasing the temperature results in a decrease of the $\left(0, \frac{1}{2}\sqrt{2}, 0\right)$, $\left(1, \frac{1}{2}\sqrt{2}, 0\right)$ and the $\left(2, \frac{1}{2}\sqrt{2}, 0\right)$ peak in the spectrum. Those peaks show the (2×1) ordering of the $Cu_{50}Pd_{50}$ terminated (110) surface. The intensity of the $\left(0, \frac{1}{2}\sqrt{2}, 0\right)$ peak is given as function of the temperature in fig. 16. The intensity of the peak gets smaller in the temperature trajectory 200-260K. Above a temperature of ~260K the order has disappeared.

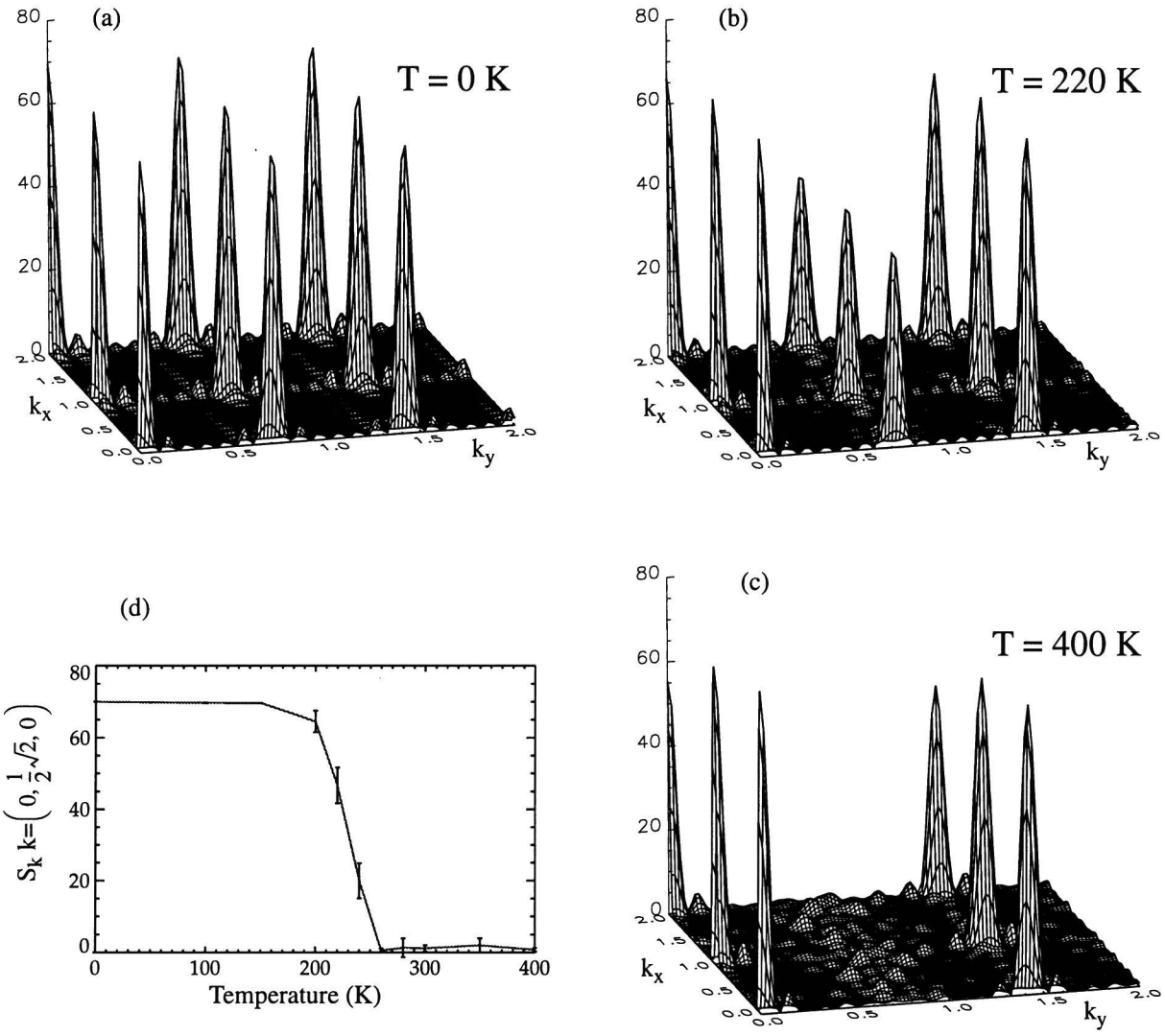

- Figure 16 - The structure factor, S(k), as defined in Eq. (39) computed for the (110) surface. The peaks in (c) show order in lattice positions. Cooling down to a temperature of 0 K peaks appear (a). In (d) the k=$\left(0, \frac{1}{2}\sqrt{2}, 0\right)$ peak is shown as function of temperature. The k_x and k_y vector are in units of (2π/a) with a the lattice parameter.

4.5. Simulations of the TOF-SARS experiments

Molecular dynamics simulations are performed of the TOF-SARS experiments on $Cu_{85}Pd_{15}$(110) and Cu(110) surfaces. The TOF-SARS spectrum of $Cu_{85}Pd_{15}$ (110) with the original assignments of the peaks is shown in fig. 8a on page 7. The aim of the simulations is to assign the different peaks in the TOF-SARS spectra to scattering or recoil processes. In order to do so, MD simulations have been carried out of the bombardment with 1.5 keV Ar^+ ions on Cu terminated and $Cu_{50}Pd_{50}$ terminated Cu_3Pd surfaces. Also simulations have been carried out on a Cu(110) surface with different angles of incidence.

In the simulations, a non-reconstructed (110) surface of a fcc microcrystallite that consists of 4 layers of 24 atoms per layer is used. Periodic boundary conditions parallel to the surface are applied in order to minimize boundary effects. The size of the microcrystallite is sufficiently large to prevent interference due to the periodic boundary conditions and its finite size parallel to the surface. The bottom layer atoms are coupled to their initial positions with an harmonic force. The value of the force constant is 155 Nm^{-1}.

For each case, a set of trajectories is developed by uniform sampling of a representative area reflecting the underlying symmetry of the surface. With every new trajectory, a fresh surface is bombarded with the projectile. The simulations produce quantitative, time-resolved information of the motion of all atoms in the crystallite and are continued for the time that a scattered ion or recoil atom needed to escape from the surface. Statistical information is obtained on the velocities of the scattered ions and recoil atoms.

4.5.1. Cu_3Pd(110)

The first simulations are carried out in order to determine the possibility to discriminate between a Cu terminated and $Cu_{50}Pd_{50}$ terminated surface of a Cu_3Pd(110) crystal with the TOF-SARS technique. Cu_3Pd has been chosen in favor of $Cu_{85}Pd_{15}$ as the latter cannot have perfect ordered surfaces due to the lack of stoichiometry.

The angle of incidence is 17.5^0 with respect to the surface plane, the azimuthal angle is along the [-114] direction of the (110) surface. In fig. 17 the results are shown of the simulations for the two different terminations of the (110) surface. The flight times are displayed with an offset in the time scale so to obtain a good match with the experiments for peaks at small flight times (which are due to scattered Ar^+ ions). From the simulations it can be observed that the main difference between the two figures is the contribution of Pd at large flight times. Unfortunately, detection at large flight times appears to be impossible with the current experimental set up. From the simulations it is observed that the peak at the smallest flight times corresponds to multiple scattering of the Ar^+ ions on Cu and/or Pd atoms. The peak at t~12μs is due to Cu recoil atoms and the peak at t~19μs is due to Pd recoil atoms.

The large experimental peak at t~9μs is not observed in the simulations.

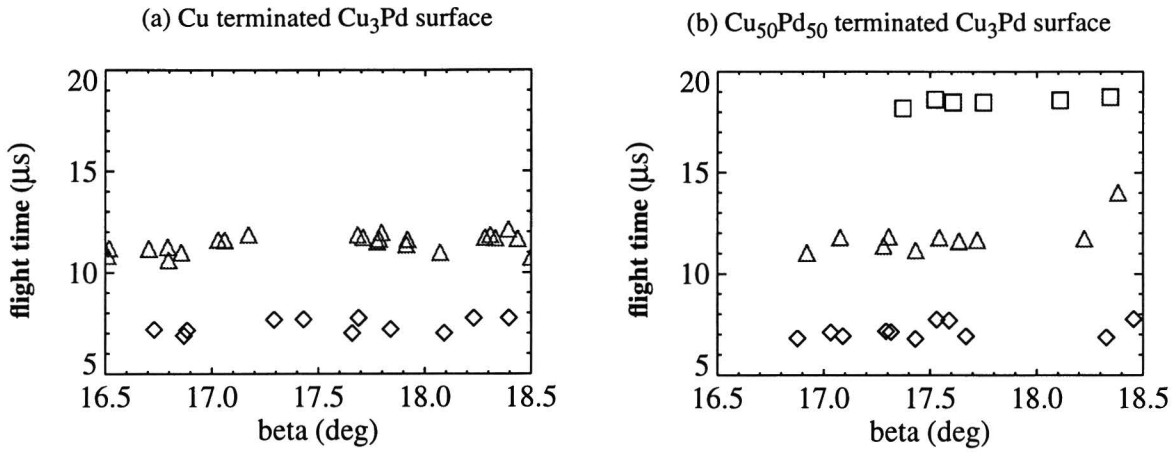

- Figure 17 - Simulated TOF-SARS experiment of a $Cu_3Pd(110)(2x1)$ surface. Diamonds: Ar, triangles: Cu and squares Pd. A diamond at beta=17.4^0 and flighttime=7μs represents a scattered Ar ion with exit angle 17.4^0 with respect to the surface plane, that had a time-of-flight of 7μs.

4.5.2. Cu(110)

In order to check the computer simulations on its ability to obtain agreement with experimental data, experiments and simulations are carried out with a single crystalline Cu(110) surface. This surface is known to have a non-reconstructed (110) surface and is well suited for the comparison of experiments and simulations.

In both the experiments and simulations the angle of incidence is 17.5^0 with respect to the surface plane. Two cases are investigated: one with the azimuthal angle along the [-114] direction of the (110) surface and the second with a 6 degrees offset from the [-114] direction towards the [001] direction.

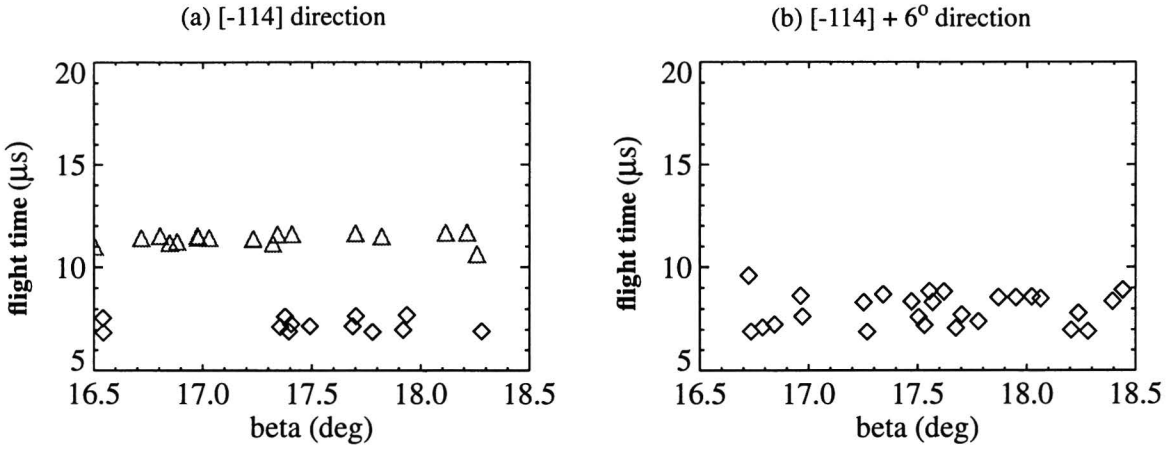

- Figure 18 - Simulated TOF-SARS experiment. Diamonds: Ar and triangles: Cu.

The experimental TOF-SARS spectrum of the first case is very similar to the experimental spectrum of $Cu_{85}Pd_{15}(110)$ and shows a considerable peak originating from Cu recoils. However, a peak at t~9μs is not observed in the spectrum. In the second case, with the 6 degrees offset from the [-114] direction towards the [001] direction, the amount of Cu recoils has become very small. In de TOF-SARS spectrum a peak appears at t ~ 9μs that is larger than the Cu recoil peak.

The simulation data are shown in fig. 17. It is clearly demonstrated that also in the simulations a large peak appears at t~9μs. It is now possible to investigate the origin of this peak. In fig. 19 one of the trajectories is visualized of an Ar^+ ion that contributes to the peak at t ~ 9μs. When the azimuthal angle is such that an surface atom can be hit at the side, the ion will continue its trajectory horizontally until it is scattered from a next atom and finally escapes from the surface towards the detector. When the azimuthal angle is along the [-114] direction, the shadow cones of other atoms prevent this process from taking place.

The way to obtain the t ~ 9 μs peak is to hit the surface atoms low enough to make the trajectory possible visualized in fig. 19. The t ~ 9 μs peak in the $Cu_{85}Pd_{15}$ TOF-SARS spectrum can not be caused by an 6 degrees offset from the [-114] direction because in that case the Cu recoil-peak will become very small. The recoil peak in the TOF-SARS experiments is a maximum as can been seen in fig. 8a on page 7.

The shadow cone which prevents the Ar^+ ion from hitting the surface atom at the side is caused by another surface atom. Removing this atom will result in a possibility for a scattering process that contributes to the peak at t ~ 9 μs. The conclusion is that the surface must have a missing row structure, a high step density or a lot of vacancies. A missing row construction was ruled out because of the TOF-SARS spectrum as explained in paragraph 2.2. on page 8. Therefore we investigate the properties of a surface containing vacancies.

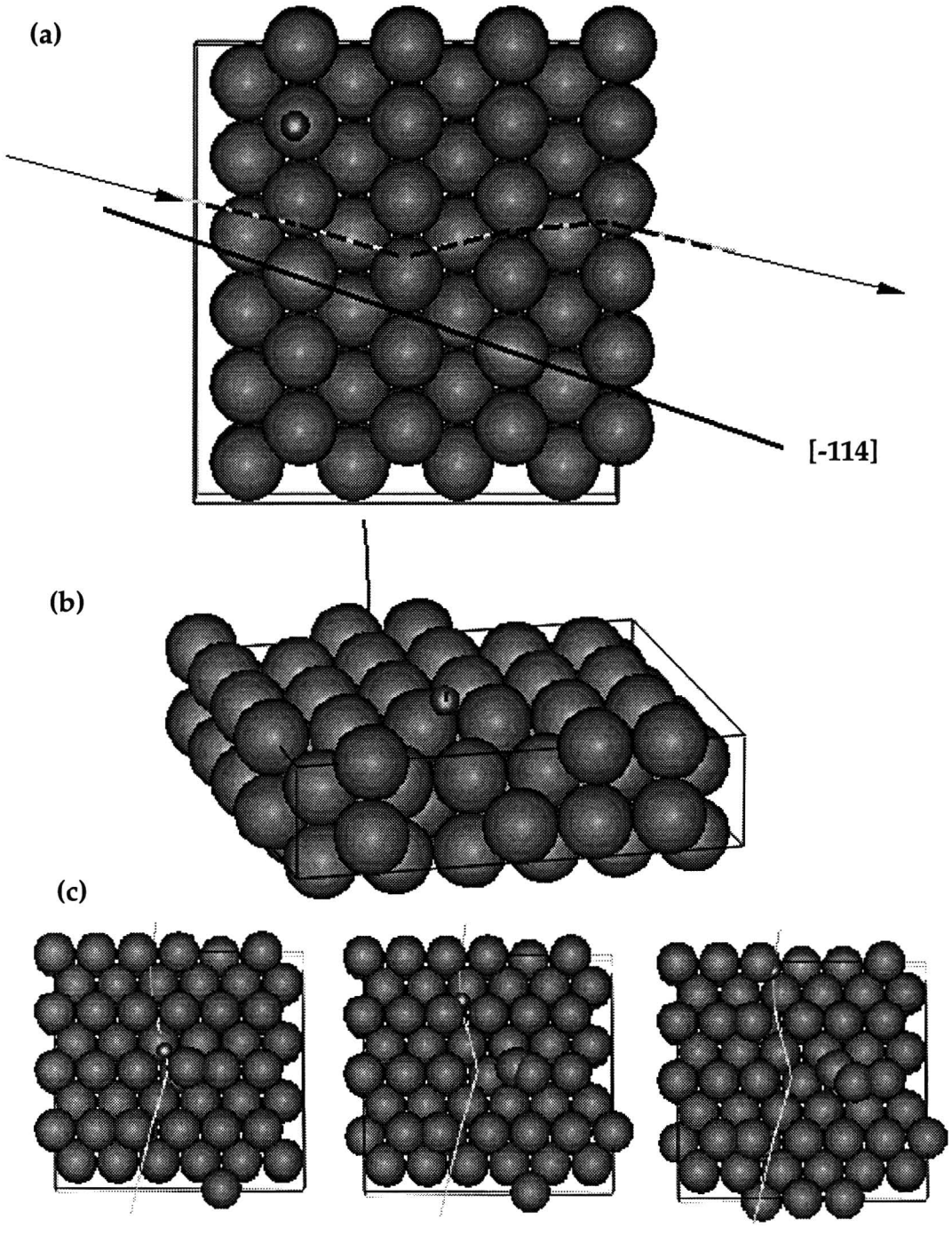

- Figure 19 - Trajectory of a scattered Ar^+ ion that has a flight time of approximately 9μs. The large spheres are Cu atoms, the small sphere is the Ar^+.

4.6. Behavior of vacancies in the surface

Monte Carlo simulations are performed to investigate the behavior of vacancies in the (110) surface. The simulation method is similar with the method used in the surface simulations in paragraph 4.4. The composition of the alloy is controlled with the chemical potentials of the elements. The simulation cell contains 4608 atoms. The number of layers is 24 and each layer consists of 192 atoms. The vacancies are treated like atoms which have no interaction with other atoms. Because the number of vacancies has to be fixed, another procedure for the configurational changes of the simulation cell is followed. An atom is chosen at random in a Monte Carlo step. If this atom is a Cu or Pd atom the procedure as described in paragraph 3.2.1. on page 12 is followed. In the case that a vacancy 'atom' is chosen, a second surface 'atom' (Cu or Pd atom or a vacancy) will be chosen at random and the two 'atoms' will be exchanged.

The first simulation is carried out in order to investigate the general behavior of the vacancies. Initially one surface termination consists of 100% copper atoms. Half of the surface atoms is exchanged with vacancy atoms. The vacancies are distributed uniformly over the surface. The other surface has a $Cu_{50}Pd_{50}$ composition. Half of the Cu atoms and half of the Pd atoms are exchanged for vacancies. The number of vacancies is 50% because we want to allow the surface to form a missing row construction.

(a) Simulation after 25 million MC steps.

(b) Simulation after 50 million MC steps.

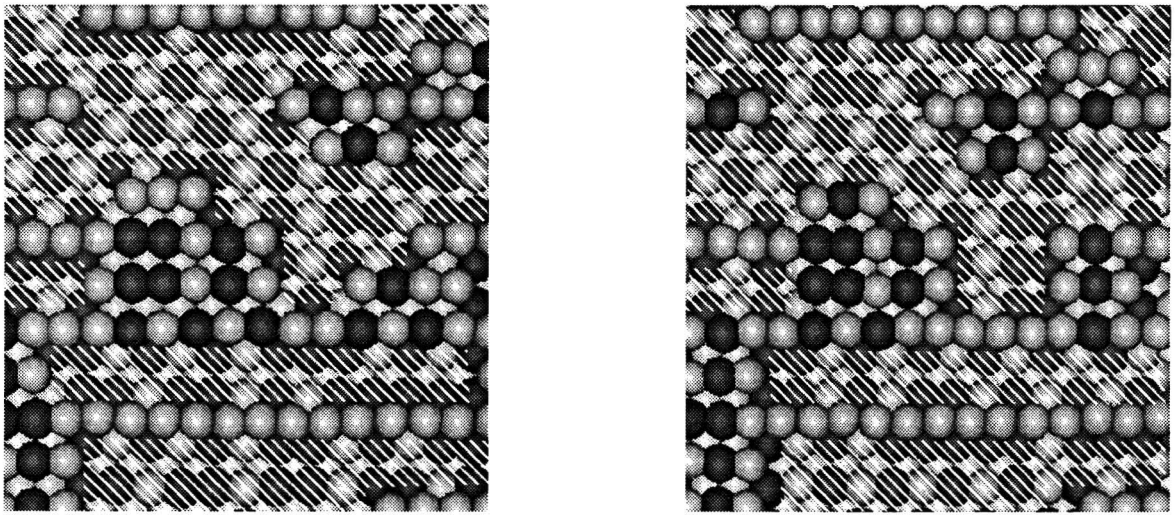

- Figure 20 - A Monte Carlo simulation to simulate the behavior of vacancies in the surface. The initial surface contains 50 at.% vacancies equally distributed over the surface. The shaded part corresponds to the final vacancy distribution.

After 25 million MC simulation steps at a temperature of 200K the configuration is like fig. 20 . The general trend is missing row and island forming on the surface. Continuing the simulation for another 25 million Monte Carlo steps does not change the structure much. The composition shows a small change. The rows which form the missing row constructions are strongly enriched with copper. The islands on the surface seem

to have a $Cu_{50}Pd_{50}$ composition. From the island formation can be concluded that there will be no individual vacancies in the surface because the vacancies will diffuse to the steps.

4.6.1. Missing row structure

The missing row structure is investigated using a simulation cell with two surfaces. One surface is a 100% Cu surface where half of the rows are removed to construct the missing row structure. The outermost layer of this surface will not show any changes in structure and just a small change in composition during the simulation. The second layer of this surface, which initially contained 50 at.% palladium and 50 at.% copper atoms will have a small enrichment in palladium in equilibrium. The second layer consists ~ 65 at.% Pd at a temperature of 200K.

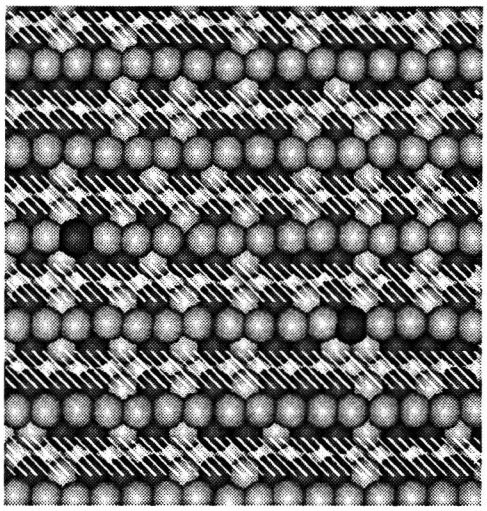

- Figure 21 - The initial cell of this simulation has a [110] Cu_3Pd missing row surface with 100% Cu in the outermost layer. This is the configuration after 25 million MC steps at a temperature of 200K. The shaded part correspond to the missing rows.The dark atoms are the palladium atoms The other atoms are copper atoms.

The other simulated surface was a $Cu_{50}Pd_{50}$ surface initially. Half of the rows was removed again to construct a missing row structure. The structure is stable during the simulation. In equilibrium the rows on the surface will be enriched with copper and the final composition of the second layer will be ~65 at.% Pd and ~35 at.% Cu.

The surface energy of missing row surfaces is calculated. At a temperature of 0 K the surface energy of the Cu terminated missing row surface is $\gamma_{initial}$=1.42 J/m^2. In case the atoms in the outermost layers were free to relax the surface energy is γ_{relax}= 1.36 J/m^2. The $Cu_{50}Pd_{50}$ terminated missing row surface gives an surface energy of $\gamma_{initial}$=1.47 J/m^2 and after relaxation γ_{relax}=1.42 J/m^2. The missing row reconstructed 100% Cu terminated surface and the unreconstructed $Cu_{50}Pd_{50}$ terminated surface have the same surface energy.

4.6.2. Stepped surface

The existence of the t ~ 9 μs peak may also be explained with a stepped surface or an island structure on the surface. The Ar^+ ions in the TOF-SARS experiments can hit the atoms on the step without being disturbed by the shadow cones of other atoms. Monte Carlo simulations have been performed to investigate the stability of the step. Initially one surface of the simulation cell is constructed of 100% copper atoms. In order to create a step on the surface, half of the atoms is exchanged for vacancy 'atoms'. The result is a surface with half of the outermost layer $Cu_{50}Pd_{50}$ and half of the surface consisting of 100% Cu. The other surface is a $Cu_{50}Pd_{50}$ surface initially. Half of the atoms is exchanged with vacancies as well.

(a) Initially the shaded part was $Cu_{50}Pd_{50}$ and the other part 100% Cu

(b) Initially the shaded part was 100% Cu and the other part $Cu_{50}Pd_{50}$

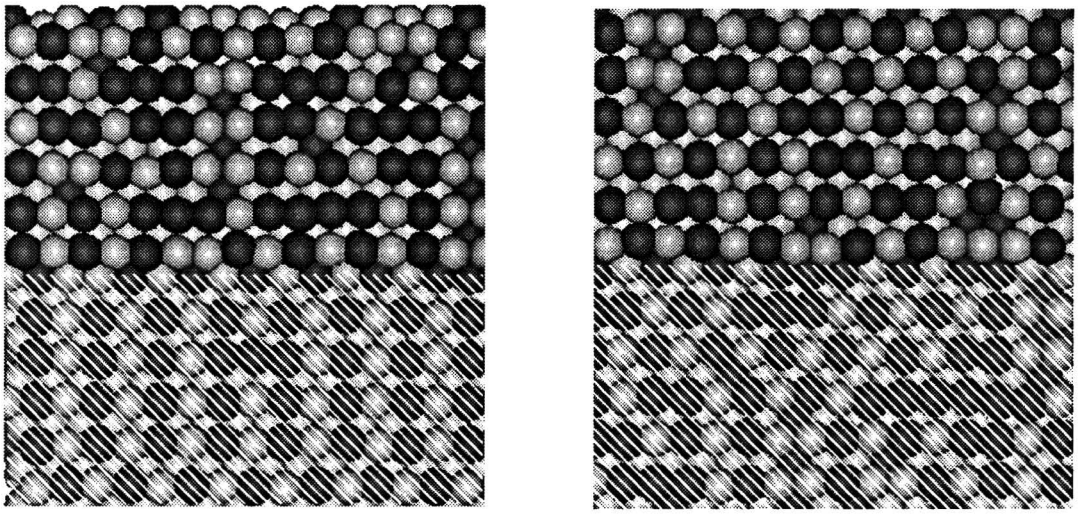

- Figure 22 - Simulation of surface with one step at a temperature of 200 K. The bulk structure is Cu_3Pd. The dark atoms are the palladium atoms The other atoms are copper atoms.

In equilibrium the surface parts with 100% copper initially are enriched with Pd until a composition with ~50 at.% Pd is reached. The $Cu_{50}Pd_{50}$ parts of the surface will keep the same structure. The second layer will be enriched with copper. The surface configurations after 25 million simulation steps are shown in fig. 22. Surface energy calculation at a temperature of T ~ 0K is not possible in this case because the underlying structure is unknown.

The composition of the step edge was investigated as function of the temperature. The row atoms at the step edge has a small enrichment of copper. The row consists of ~55 at.% Cu and ~45 at.% Pd. The row just beneath this step edge has the same composition as the rest of the surface, which means ~50 at.% Cu and ~50 at.% Pd. The composition of the step edge on the surface is not temperature dependent at temperatures between 100 K and 400 K.

5. CONCLUSION

The outermost layer of the $Cu_3Pd(110)$ surface has a $Cu_{50}Pd_{50}$ composition at a temperature of T=0K. The second layer consists of 100% Cu. The calculated surface energy of the $Cu_{50}Pd_{50}$ terminated surface is $\gamma = 1.36\,J/m^2$.

The Monte Carlo simulations of the $Cu_3Pd(110)$ crystal surface show the same termination for low temperatures. The $Cu_{50}Pd_{50}$ layer is ordered. The order-disorder transition temperature of the $Cu_{50}Pd_{50}$ terminated surface is T~220K. The surface order-disorder transition temperature is lower than the bulk order-disorder transition temperature because the atoms in the surface are less bounded than the bulk atoms. Therefore the surface atoms will be less restricted to move. Above the order-disorder temperature the second layer of the $Cu_{50}Pd_{50}$ terminated surface shows a small enrichment in Pd of ~10at.%. The $Cu_{50}Pd_{50}$ terminated surface can not be ruled out by the TOF-SARS experiments. The detector is not able to measure the Pd recoil atoms, because of their low kinetic energy. The EARISS experiments are in contradiction with the simulations because those experiments show ~11at.% Pd in the outermost layer and ~40at.% Pd in the second layer.

A peak which was not mentioned in the TOF-SARS spectrum can be assigned to a result of an scattering process low in the surface. This is only possible in case vacancies are existent in the surface.

Monte Carlo simulations which allow vacancies in the surface show that the vacancies will group. The resulting configurations are a missing row reconstructed surface or a stepped surface. The outermost layer of the missing row reconstructed surface contains 100% Cu atoms. The surface energy of this structure is $\gamma = 1.36 J/m^2$ at a temperature of T~0K. The missing row reconstruction is ruled out because this structure is in contradiction with the TOF-SARS experiments. The stepped surface is also a stable configuration with a $Cu_{50}Pd_{50}$ terminated surface. The step density has to be very high to cause a large peak at t~9μs.

It can be concluded that using the EAM potentials the surface will be a missing row reconstructed surface with 100% Cu in the outermost layer or a $Cu_{50}Pd_{50}$ stepped surface with a high step density. Both configurations are in poor agreement with the experimental results. Despite the good agreement between literature and calculations for the bulk situation a good agreement of the surface properties is not obtained with this method. Therefore care must be taken in the interpretation of the simulation results.

This work strongly suggests that the number of defects in the $Cu_{85}Pd_{15}(110)$ (2×1) surface is very large. The structure of the surface has to be investigated further for example by SPA-LEED or STM. The crystal used in the experiments by Bergmans may have a large miscut. The large number of defects in the surface can also be a result of the anneal temperature. In case that the anneal temperature in the experiments is too low, islands can appear on the surface.

It can be very useful to increase the sensitivity of the TOF-SARS detector for larger flight times because the kinetic energy of the recoils of the Pd element is too low to be detectable with this setup. This problem can simply be solved by increasing the kinetic energy of the ions in the experiments.

Another suggestion for further investigation is the calculation of the ratio between the number of Cu recoil atoms and the number of Ar^+ scattered ions in the t~9μs peak in the TOF-SARS spectra. The result of this calculation is probably a value which represents the number of steps on the surface. If this is true, the TOF-SARS can be used as a sensitive technique to measure the step density and the step composition on surfaces.

References

[1] J.C. Summers and W. Burton, 205th ACS meeting, symposium on environmental catalysis, Denver (1993), paper 35

[2] M.S Daw, S.M. Foiles and M.I. Baskes, Materials Science Reports 9 (1993), 251-310, North-Holland

[3] S.M. Foiles, Physical Review B, 32, 7685 (1985)

[4] R.H. Bergmans, M. van de Grift, A.W. Denier van der Gon and H.H. Brongersma, to be published

[5] R.H. Bergmans, M. van de Grift, A.W. Denier van der Gon, R.G. van Welzenis, H.H. Brongersma, S.M. Francis and M. Bowker, Nucl. Instr. and Meth. B 85 (1994) 435 and refs. there in.

[6] K. Hansen, Constitution of binary alloys, second edition, McGraw Hill Book Company, New York, 1958

[7] W.B. Pearson, Handbook of lattice spacings and structures of metals and alloys, Pergamon Press, London, 1958

[8] M.S. Daw and M.I. Baskes, Physical Review B 29, 6443 (1984)

[9] M.S. Daw, 1990, Many-Atom Interactions in Solids (Springer Proc. Phys. 48) ed R.M. Nieminen, M.J. Puska and M.J. Manninen (New York: Springer), p 48

[10] J.H. Rose, J.R. Smith, F. Guinea and J. Ferrante, Physical Review B 29, 2963 (1984)

[11] S.M. Foiles, M.I. Baskes, and M.S. Daw, Physical Review B, 7983 (1986)

[12] E. Clementi and C. Roetti, At. Data Nucl. Data Tables 26, 197 (1981)

[13] K.Binder (editor), Monte Carlo Methods in Statistical Physics, Springer, Berlin, 1986

[14] K.Binder (editor), Application of the Monte Carlo Method in Statistical Physics, Springer, Berlin, 1984

[15] M.P. Allen and D.J. Tildesley, Computer Simulations of Liquids, Clarendon Press, Oxford, 1987.

[16] T.L. Hill, Statistical Mechanics, McGraw-Hill Book Company inc., New York, 1956

[17] K. Huang, Statistical Mechanics, John Wiley & Sons, New York, 1987

[18] S.M. Foiles and M.S. Daw, J. Mater. Res. 2 (1), Jan/Feb 1987 (5)

[19] H. Feil, J. Dieleman and B.J. Garrison, J. Appl. Phys. 74 (2), 15 July 1993

[20] S.M. Foiles, Physical Review B, 49, 14930 (1994)

[21] A.A. Maradudin, E.W. Montroll and G.H. Weiss, Theory of Lattice Dynamics in the Harmonic Approximation, 2nd ed. (Academic, New York, 1971)

[22] B.E. Warren, X-ray diffraction, Addison-Wesley Pub. Co., 1969

[23] A.Garcia and J.E. Northrup, J. Vac. Sci. Technol. B 12(4), Jul/Aug 1994 (2678)

[24] A.R. Miedema, Z. Metallkde., 69 (1978), H. 7

Acknowledgements

Dr. A.W. van der Gon stimulated me to investigate the surface of an alloy with computer simulations and started a cooperation with Dr. H. Feil.

My special thanks goes to Dr. H. Feil for performing the Molecular dynamics simulations, the numerous of valuable discussions and the advice he gave me. It was very pleasant to work with him.

Drs. J.C.J. Paasschens shared his room with me and I enjoyed his company and discussions. I also enjoyed the company of the other members of the group Experimental and Theoretical Physics of Prof.dr. H. van Houten.

I would also like to thank Philips Electronics N.V. in Eindhoven for giving me the opportunity to do this work at the Philips Research Laboratories. Financial support of Philips is acknowledged.

Appendix A: Embedded Atom Method potential functions for Al-Cu Alloys

A.1. Introduction

Since interconnects make up a large fraction of the area of an IC, reducing the average interconnect widths allows use of a greater number of devices per unit of circuit area. Increasing the number of devices per unit of circuit area, and therefore a reduction of the transmission distances, leads to an increase of the achievable speed of operation of the IC. Unfortunately, the ability to implement these designs is currently limited by reliability concerns, due primarily to electromigration.

Electromigration is electronic current induced atomic diffusion. Because of the smaller dimensions of the interconnects, the current density in the conductor increases. At current densities as high as those used in integrated circuits ($\sim 4 \times 10^5$ A/cm^2) there is enough transfer of momentum from the electrons to the atoms of the conductor to cause a biased atomic self-diffusion in the direction of the electron transport. The result is a net flux of atoms in the direction of the electron flow and a net flux of the vacancies in the opposite direction. The diffusion of the conductor atoms can lead to voids in the interconnects. The growth and coalescence of voids can eventually lead to open circuit failure.

The problem of diffusion of conductor atoms is minimized by the addition of small amounts of copper (~1 at.%) to the aluminum. However, there is no clear understanding of the role of the Cu atoms in the Al interconnects. Therefore theoretical work needs to be done to investigate the Cu behavior in the Al, especially grain-boundary segregation of Cu in Al because the interconnects consists of Al grains. In this investigation Monte Carlo and Molecular Dynamics simulations will play a crucial role. These simulations make use of interatomic potentials. A set of embedded atom method (EAM) potentials is developed by Rohrer [A1]. The potentials developed by Rohrer describe dilute Al-Cu-Ag alloys, but they are not capable to describe experimental observed ordered phases.

In this work the Al-Cu potential functions will be improved by extending their applicability to an experimental observed ordered phase, the θ phase. From experiments it is observed that θ is the precipitate which nucleates and grows at grain boundaries.The improvement of the Al-Cu potential functions is done by a least-square fit of the free energy of the bulk calculated as a function of the lattice parameter to Augmented-spherical-wave (ASW) [A2] calculations performed by H. Feil.

In the next paragraph a small overview of the AlCu alloy is shown. In paragraph 3 the EAM potential functions by Rohrer will be discussed and in paragraph 4 the results of the fitting will be discussed.

A.2. Overview

The phase diagram of the Al-Cu alloy for small atomic percentages of copper is shown in fig. 23 [A3]. The composition of interest for this work contains ~1 at.% Cu. At low Cu percentages there are two structures possible, Al in a fcc lattice with randomly Al atoms exchanged for Cu atoms, or regions of Al_2Cu θ phase in an Al fcc bulk.

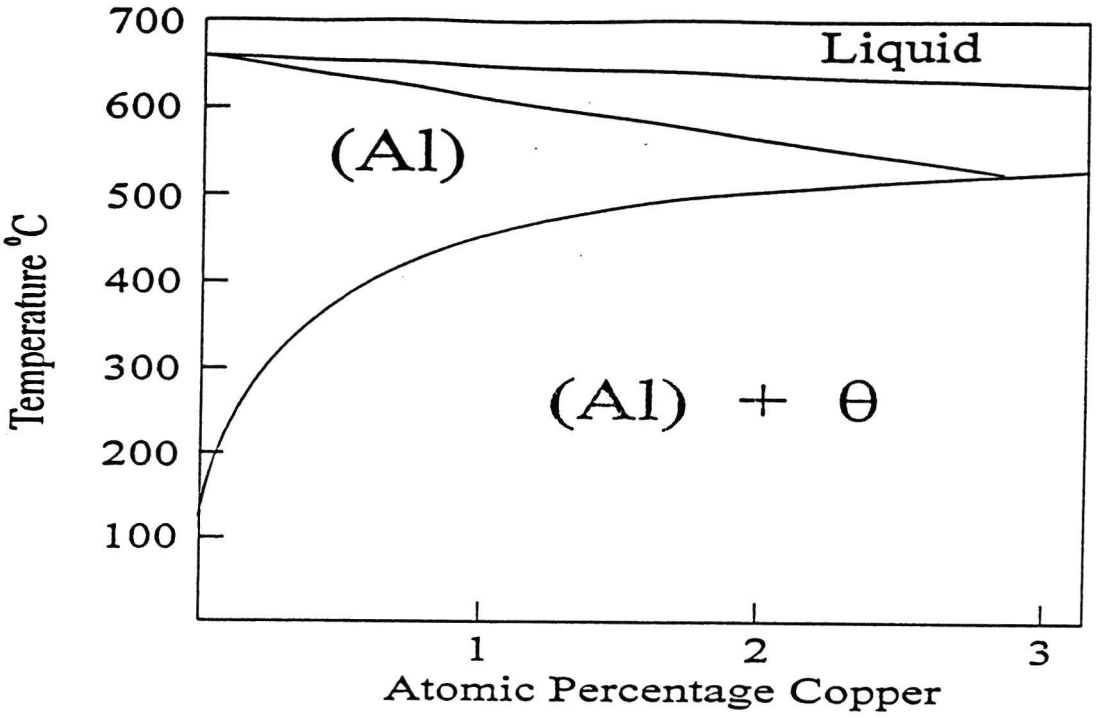

- Figure 23 - Phase diagram of an Al-Cu alloy [A3].

From experiments it is known that at the grain boundaries the Al_2Cu θ phase arises [A4]. The structure of the θ phase in Al-Cu is shown in fig. 24.

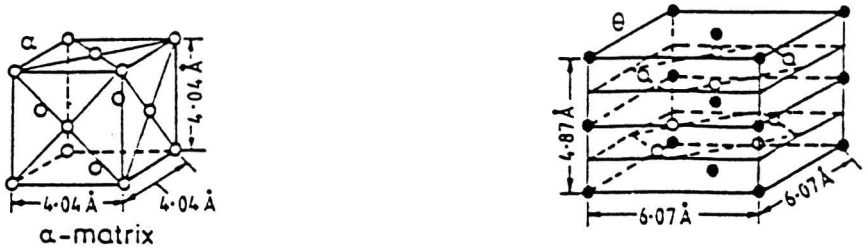

- Figure 24 - The structure of the fcc (α) and the Al_2Cu θ phase. The dark atoms are Cu, white Al [A4].

A.3. Embedding Atom Method potentials for Al-Cu

The potentials used to describe the interactions between the aluminum and copper atoms are the Embedded Atom Method potentials. In this approach, the energy of the metal is viewed as the energy obtained by embedding an atom in the local electron density provided by the remaining atoms of the system. This results in a contribution of many- body interactions in the calculation of the total energy of the metallic system.

The total energy of the system is described as a sum of the energy (F_i) necessary to embed an atom in the local density (ρ_i) and a pair interaction term (Φ_{ij}):

$$E_{tot} = \sum_i F_i(\rho_i) + \sum_{i,j>i} \Phi_{ij}(r_{ij}) \tag{40}$$

where F_i only depends on the element of atom i. For the local electron density a linear superposition can be made of the electron densities from atom i at distance r given by

$$\rho_i = \sum_j \rho_j^a(|r_i - r_j|) \tag{41}$$

In this equation ρ_j^a is the electron density of the remaining atoms. The parameterized functions of the electon density where taken from Rohrer [A1]. The electron density function used for each type of atom type is shown as follows:

$$\rho_i^a(r) = c_i\left[r^{\kappa_i}\exp(-\beta_i r) + 2^{(\kappa_i+3)} r^{\kappa_i}\exp(-2\beta_i r)\right] \tag{42}$$

The pair interaction used is in the form of the Morse potential shown as follows:

$$\Phi_{ij}(R_{ij}) = D_{ij}\left[\exp(-2\alpha_{ij}(r_{ij}-R_{ij})) - 2\exp(-\alpha_{ij}(r_{ij}-R_{ij}))\right] \tag{43}$$

To be suitable for use in Molecular dynamics and Monte Carlo simulations, the interatomic potential and its first derivatives with respect to their nuclear coordinates need to be continuous at all geometries of the system. Therefore we force the pair potential and the electron density to be zero at this cut-off distance by defining a smoothing function [A5]

$$f_{smooth}(r) = f(r) - f(r_{cut}) + \frac{r_{cut}}{m}\left[1 - \left(\frac{r}{r_{cut}}\right)^m\right]\left(\frac{df}{dr}\right)_{r=r_{cut}} \tag{44}$$

where f(r) denotes $\Phi(r)$ or $\rho(r)$ and m=20. The cut-off distance (r_{cut}) is used in the fitting procedure as well. When the pair interaction and the electron density functions are defined, the embedding energy can be found from the universal equation defined by Rose et al. [A6].

Fitting these functions with a least-squares fit of calculated material properties to experimental values led to the parameters given in Table 3. The experimental values are: the anisotropy ratio, the shear modulus, the bulk modulus, the vacancy formation energy and the intrinsic stacking fault energy. The potential functions for each element were fitted independently of one another by adjusting the like pair interaction parameters D_{ij}, α_{ij} and R_{ij} and two of the three electron density parameters, κ_i and β_i, with the c_i values held

constant. Like pair interaction parameters are the parameters in the potential function describing the interaction of elements with the same chemical identity. Unlike pair interaction parameters are the parameters in the pair interaction function of elements with different chemical identity. The scaling factors c_i in the electron density function and the unlike pair interaction parameters D_{ij}, α_{ij} and R_{ij} are determined by fitting to the dilute heats of solution of the binary alloy and to volume relaxations caused by impurities.

Table 3: Best-fit Morse potential and electron density function parameters for Al and Cu.

	Al-Al	Cu-Cu	Al-Cu
D_{ij} (eV)	1.0245	0.9721	1.6515
R_{ij} (A)	2.1608	2.2158	2.2418
$\alpha_{ij}(A^{-1})$	1.3066	1.3099	1.9507
$\beta_i(A^{-1})$	2.9562	3.0672	---
κ_i	10.2137	6.6651	---
c_i	0.0400	2.9341	---
r_{cut} of Φ_{ij}(A)	5.55	4.91	6.55
r_{cut} of ρ_{ij}(A)	6,55	4.91	---

A.4. Fitting results and discussion

The goal of this work is to extend the Al-Cu potential functions of Rohrer to potentials which are capable to describe the Al_2Cu θ phase. Only the parameters of the potential functions which concern the Al-Cu interaction are refitted. The parameters which will be varied during the fit are the unlike pair interaction parameters D_{ij}, α_{ij} and R_{ij} of Al-Cu. The parameters are fitted to the ASW calculations performed by H. Feil. The total energy of a Al_2Cu θ unit cell containing 12 atoms is obtained from these ASW calculations as a function of the lattice parameter. The axial ratio (c/a) of the θ unit cell is kept constant in the calculations. The results of the ASW calculations at 7 lattice parameters is shown in Table 4.

The fitting is done by minimization of the least-squares function χ:

$$\chi = \sum_{p} [E_{fit}(a(p), D_{ij}, \alpha_{ij}, R_{ij}) - E_{ASW}(a(p))]^2 \qquad (45)$$

In this equation $E_{ASW}(a(p))$ is the energy at lattice parameter a(p) calculated with the ASW calculations (Table 2). $E_{fit}(a(p),D_{ij},\alpha_{ij},R_{ij})$ is the energy for this lattice calculated with the EAM potential functions.

Table 4: ASW calculations of the Al_2Cu θ phase as a function of lattice parameter.

a(p) in (A)	$E_{ASW}(a(p))$ in (eV)	a(p) in (A)	$E_{ASW}(a(p))$ in (eV)
5.90	-42.3124	6.15	-42.6222
5.95	-42.5188	6.20	-42.4934
6.00	-42.6476	6.25	-42.3120
6.07	-42.7078		

Therefore a code is developed which minimizes the function χ. A subroutine calculates the total energy ($E_{fit}(a(p),D_{ij},\alpha_{ij},R_{ij})$) of a cell with atoms with an Al_2Cu θ structure as a function of the unlike pair interaction parameters $D_{ij},\alpha_{ij},R_{ij}$ and the lattice parameter. The parameters are adjusted until the function reached a minimum. The minimization method is called the Powell's method [A7]. In this method, the function is minimized for one variable. From this point the method goes on with another variable. The function is minimized for this variable and so on until the function stops decreasing.

The initial parameters of this least-square fit are shown in Table 3, D_{ij} = 1.6515, R_{ij} =2.2418 and α_{ij} = 1.9507. The final parameters are D_{ij} = 1.4787, α_{ij} = 2.2854, R_{ij} = 1.8879. The value of χ at the end of the fit is χ ~ 300. Initially the χ was ~ 3300. The free energy of the Al_2Cu θ phase with the fitted parameters is Eθ = -41.94 eV in equilibrium. The random distribution of the Al and Cu atoms on a fcc lattice gives a lower free energy (E_{fcc} = -42.68 eV). Initially these values were Eθ = -42.81 eV and E_{fcc} = -43.30 eV. The value of Eθ in the ASW calculations is Eθ = -42.71 eV in equilibrium. The energy difference between Eθ and E_{fcc} for the potential functions by Rohrer was 0.49 eV. In case of the fitted parameters the energy difference is 0.74. The difference became larger instead of smaller and therefore it makes no sense to continue this procedure.

There are two opportunities left which can be tried. One opportunity is to force the free energy of the θ phase to be lower than the free energy of the fcc phase, the free energy of the fcc lattice in equilibrium is included in the fit. The result is an extra constant to fit on, the free energy of the fcc phase at the equilibrium lattice parameter. In literature it is reported that the Al_2Cu θ phase is stable below a temperature of ~900K. Below this temperature the crystal is ordered. Above this temperature the alloy melts. The random distribution of Al and Cu atoms on an fcc lattice at this composition includes a configurational entropy term. The configurational entropy (S_{conf}) is calculated with

$$S_{conf} = -Nk_B [x_{Al} \ln (x_{Al}) + x_{Cu} \ln (x_{Cu})] \quad (46)$$

where N is the number of atoms and x is the atomic fraction of a compound. The free

energy of the θ phase should be at least TS_{conf} lower than the fcc free energy with T ~ 900K because the configurational term of an ordered state is zero.Preliminary results are not very hopeful.

The other opportunity is to vary the scaling parameters (c_i) of the electron density function during the fit procedure. The result is an extra fitting parameter to obtain a better fit. The variation of this parameter will not result in a change of the pure metal potential function parameters, because scaling the electron densities does not change the the embedding energies of the pure elements.

References

[A1] C.L. Rohrer, Modelling Simul.Mater. Sci. Eng. 2 (1994) 119-134

[A2] A.R. Williams, J. Kubler and C.D. Gelatt, Jr., Physical Review B 19, 6094 (1979)

[A3] H.E. Boyer and T.L. Gall (editors), Metalls Handbook, American Society for Metals, New York, 1985

[A4] D.A. Porter and K.E. Easterling, Phase transformations in metals and alloys, Von Nonstrand Reinhold

[A5] V. Vitek and D.J. Srolovitz (editors), Atomistic Simulation of Materials, Plenum Press, New York, 1989

[A6] J.H. Rose, J.R. Smith, F. Guinea and J. Ferrante, Physical Review B 29, 2963 (1984)

[A7] W.H. Press, S.A. Teukolsky, W.T. Vetterling and B.P. Flannery, Numerical Recipes, Cambridge University Press, 1986